Accepted Manuscript

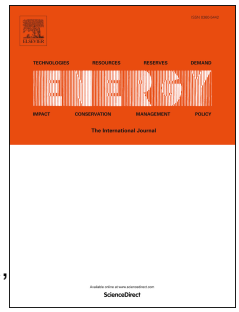

Fluids selection and performance analysis of a polygeneration plant with exergy recovery from LNG-regasification

Antonio Atienza-Márquez, Joan Carles Bruno, Atsushi Akisawa, Masayuki Nakayama, Alberto Coronas

PII: S0360-5442(19)30683-8

DOI: https://doi.org/10.1016/j.energy.2019.04.060

Reference: EGY 15089

To appear in: *Energy*

Received Date: 27 September 2018

Revised Date: 7 February 2019

Accepted Date: 9 April 2019

Please cite this article as: Atienza-Márquez A, Bruno JC, Akisawa A, Nakayama M, Coronas A, Fluids selection and performance analysis of a polygeneration plant with exergy recovery from LNG-regasification, *Energy* (2019), doi: https://doi.org/10.1016/j.energy.2019.04.060.

Fluids selection and performance analysis of a polygeneration plant with exergy recovery from LNG-regasification

Antonio Atienza-Márquez [a,] *, Joan Carles Bruno [a], Atsushi Akisawa [b], Masayuki Nakayama [b], Alberto Coronas [a]

[a] Universitat Rovira i Virgili, CREVER – Group of Applied Thermal Engineering, Mechanical Engineering Department, Av. Països Catalans 26, 43007 Tarragona, Spain

[b] Tokyo University of Agriculture and Technology, Graduate School of Bio-Applications and Systems Engineering, 2-24-16, Nakacho, Koganei, Tokyo 184-8588, Japan

*Corresponding author: antonio.atienza@urv.cat

Abstract

Liquefied Natural Gas (LNG) is a valuable exergetic source due to its low-temperature (-162^{o}C). However, LNG is regasified using seawater as heat source and without exergy recovery in most of LNG terminals worldwide.

In this paper we model a polygeneration plant that recovers the low-temperature and pressure exergy from LNG-regasification to generate simultaneously power and refrigeration in a District Cooling network at three different temperature levels. The plant is divided into different subsystems arranged in cascade. The objective of this research is the selection of the most suitable working fluids and heat transfer fluids for operating in each subsystem. The performance of the system is analyzed from the thermodynamic and environmental point of view.

Although neither of the candidate fluids satisfies all the desirable features, the selected fluids are: methane, carbon dioxide and propane. The plant achieves an equivalent electricity production of 125 kWh for metric ton of LNG regasified with an exergetic efficiency of 40.6%. Besides, the seawater utilized in the plant is 60% lower than the required by the common LNG regasification process and an annual emission of 75 thousand tons of CO_2 is avoided.

Keywords: Liquefied Natural Gas (LNG); LNG regasification; Physical exergy recovery; Polygeneration; Fluids selection

1. Introduction

The fight against climate change is one of the major challenges of today's society. Climate agreements as the Kyoto protocol [1] aims to control the greenhouse gas emissions and mitigate the global warming. Although renewable energies contribute to this purpose, energy outlooks predict that fossil fuels will remains as the main source of primary energy in the decades to come; despite the greater share of renewable energies in the primary energy mix and the deaccelerated growth rate of oil and coal [2]. In these forecasts, Natural Gas (NG) highlights as the only fossil fuel whose share in the primary energy mix increases, assuming a key role in the energy transition towards a low-carbon energetic model. In fact, NG is a fossil fuel environmentally friendlier than, e.g., oil and coal because of its lower carbon footprint and a cleaner combustion [3]. Although critics distrust of NG sustainability due to methane leakages to the atmosphere along NG supply chain, conclusive data about these emissions are missing [4,5].

Although NG is usually supplied by pipelines, its long-distance transport is a problem. In this sense, Liquefied Natural Gas (LNG) is a solution. LNG, whose composition is mainly methane (around 90%), ethane and propane [6], is obtained by cooling the pre-purified NG up to 111 K (-162^{o}C). By this way, the volume of NG is reduced enough (around 600 times) to make feasible its transport in carriers of LNG tankers. Furthermore, LNG gives a higher flexibility to the natural gas trade and avoiding the energy dependency from a specific country. The demand of LNG has increased during the last years and it will continues increasing with a growing rate of 4 to 5% to 2030 [7]. By 2035, LNG will account 50% of the total natural gas trade [8]. At present, Japan remains the top LNG importer country worldwide and the growing demand of LNG from China and India is quite remarkable [7]. By the other side, Qatar is the main world LNG supplier accounting near 30% of the total LNG export worldwide, although Australia and United States are increasing significantly their LNG exports [9].

On the other hand, the NG's liquefaction process consumes high amounts of energy that could be partially recovered when LNG is regasified before being supplied to the end-users. Up to 240 kWh/t-LNG could be recovered if an ideal conversion system is used. The cryogenic temperature of LNG makes it very attractive from the exergetic point of view and it can be applied in several industrial applications [10]: electric power production [11], air-separation units [12], light hydrocarbon separation [13], CO_2 capture [14], dry ice production, seawater desalination [15], refrigeration in cold warehouses and data centers, etc. Among these applications, electric power production is the most studied. Several typologies of power cycles and configurations have been proposed [16]. For example, LNG can be used as heat sink in Rankine cycles and Kalina cycles or in air pre-cooling of Brayton cycles. Direct expansion units can be used also to convert the pressure exergy of LNG into electricity. For the future, thermoacoustic systems are a good example of emerging technologies for power production well adapted to the LNG low-temperature [17].

However, the exergy recovery from LNG-regasification in real LNG plants is not widespread. In most of these facilities, LNG is regasified in Open Rack Vaporizers (ORVs) that use seawater as heat source, so LNG exergetic potential is wasted via seawater. In fact, there are only a few real plants worldwide recovering LNG exergy and most of them are in Japan [18]. For instance, Senboku II LNG Terminal of

Osaka Gas entails a benchmark for electric power production from LNG exergy utilization [19]. On the other hand, Negishi LNG Terminal of Tokyo Gas was a pioneer plant in the utilization of the low-temperature of LNG for the refrigeration of a refrigerated warehouse [20]. In contrast with the power production, the literature dealing with the use of LNG exergy for refrigeration applications (e.g., agro-food industry or commercial sector) is scarce [21–23].

Although LNG is a gold mine from the exergetic point of view and its cryogenic temperature use has several industrial applications, *not many LNG terminals exist worldwide recovering exergy from LNG-regasification.* The reasons are the barriers that block a further implementation of LNG exergy recovery systems. Some of these barriers have non-technical nature such as the mistrust from industry holders to substitute or adapt their conventional refrigeration systems. Another bottleneck is the conflict of interests between the gas and third-party companies that could exploit the LNG exergy. However, this type of barriers could be overcome in a near future encouraged by international energetic strategies that explicitly mentions LNG-regasification as a chance of waste cold recovery (e.g., the European Strategic Energy Technology Plan (SET) [24]). Additionally, there are technical barriers to overcome such as the fluctuating refrigeration demand, for which thermal energy storages are a promising solution [25,26].

But some of the major technical barriers are related with the low efficiencies of this kind of power generation systems and the lack of suitable operating fluids. Efficiency of cryogenic power units are rarely beyond 20% [27]. In this sense, polygeneration [28,29] is a promising way for exploiting LNG physical exergy more efficiently [30,31]. Whereas most of current research is focused on exploiting LNG exergy for a single application, polygeneration allows a cascading exploitation of LNG exergy for multiple applications. In a previous work presented in Atienza-Márquez et al. [30], we proposed a novel polygeneration plant with exergy recovery from LNG-regasification for the combined production of electricity and refrigeration in a District Cooling (DC) network with three different temperature levels. But even though a diligent selection of the best operating fluids is particularly crucial for LNG exergy recovery systems, this issue was not addressed in our previous research.

There is not a fixed rule for the selection of the most suitable fluids, and many factors should be considered: the typology of the system, the heat source and heat sink temperatures, the distance between the LNG regasification site and the cold utilization site, etc. For instance, Rao et al. [32] determined that R143a, propane and propylene were the most suitable fluids for a combined power cycle that exploits solar energy and the low-temperature and pressure components of LNG exergy. Badami et al. [33] identified ethane, propane and propylene as suitable working fluids for three different combined power cycles with LNG exergy utilization and Li et al. [23] considered that R23 was the most suitable fluid for use LNG low-temperature exergy in a cold warehouse. Furthermore, many authors select CO_2 when the cold recovered from LNG has to be transported over long distances [21,22,34]. In the case of real cryogenic power cycles, propane [35] and hydrocarbon mixtures are also used [36].

The objective of this paper is twofold. The first objective is the selection of the most suitable working fluids and heat transfer fluids for a polygeneration plant based on exergy recovery from LNG-regasification for the combined production of power and refrigeration at three temperature levels. The

decisions about the most suitable fluids are based mainly on thermodynamic performance. Once the fluids are selected, the second objective is to analyze the performance of the plant from the thermodynamic and the environmental point of view. The paper is arranged as follows: In section 2, the polygeneration plant and its operation are described, its modelling and performance indicators are explained and a preliminary list of candidate fluids is shown. Afterwards, we present the results and the discussion about the fluids selection in section 3. Also, the performance of the whole plant operating with the selected fluids is analyzed. Finally, the conclusions of this research are presented in section 4.

2. A polygeneration plant for LNG exergy recovery

In this section, the polygeneration plant for exergy recovery from LNG-regasification is presented and its operation is described (section 2.1 and 2.2), its thermal model and its performance indicators are explained (section 2.3 and 2.4) and a preliminary screening of candidate working fluids and heat transfer fluids is presented (section 2.5).

2.1 Description of the polygeneration plant

Figure 1 shows the schematic diagram of the polygeneration plant for LNG exergy recovery. This plant is an evolved version of the one presented previously in Atienza-Márquez et al. [30]. This plant is engineered for operating in an area in which an industrial cluster with high refrigeration demand is located nearby to the LNG terminal. In this sense, the Spanish LNG terminal of Barcelona (41.33ºN, 2.16ºE) is a promising scenario. Nowadays, the Barcelona LNG terminal has an LNG regasification capacity of 1,950,000 Nm^3/h and count on a huge industrial and commercial area (e.g., agro-food sector) at its vicinity with high and constant refrigeration demand.

Fig. 1. Schematic diagram of the polygeneration plant with exergy recovery from LNG-regasification for polygeneration applications.

The philosophy of the proposed system is similar to that of conventional polygeneration systems. The main difference is the temperature of the exergy source to be exploited. A conventional polygeneration system exploits a high-temperature exergy source for the simultaneous production of multiple energy vectors or services. But the proposed polygeneration plant exploits the low-temperature and pressure components of exergy of the LNG to provide the following services: (1) LNG regasification; (2) Electric power production; (3) Refrigeration service in a District Cooling (DC) network at three temperature levels. Furthermore, an advantage of operating with low-temperature heat reservoirs such as ambient and cryogenic temperatures is that using the same temperature gradients between the heat source and sink, a higher thermal efficiency can be obtained in comparison with more conventional reservoirs above ambient temperature [30].

The structure of the plant is divided into four subsystems. Following the LNG flow downstream (from the LNG tanks to the city gas distribution pipeline), these subsystems are: a power unit (RC-1), a hybrid system that consists of a District Cooling (DC) network combined with a power unit (RC-2), another power unit (RC-3) and, finally, a natural gas direct expansion unit (EXP). These subsystems are arranged in series with the aim to recover the exergy from LNG-regasification in cascade. Moreover, this structure offers a great operational flexibility and allows for an independent operation of each subsystem. Next is given a more detailed description of the subsystems that integrate the polygeneration plant:

- **Power cycle RC-1**. This power cycle exploits LNG exergy at its lowest temperature level. It consists of a regenerative Rankine cycle that uses seawater as heat source and LNG as heat sink. The cycle has intermediate reheating with two expansion-stages. It operates upstream of the DC network because, although the temperature required by the end-users connected to the DC network is relatively low in comparison with a conventional DC network, it is not so low as the LNG storage temperature. Thus, the power cycle RC-1 produces electricity from exploiting the low-temperature exergy gap between LNG storage temperature and the temperature required by the DC network.

- **DC network and power cycle RC-2**. This subsystem of the plant is designed for operating just downstream of the power cycle RC-1 and combines a DC network with a power cycle. The DC network provides refrigeration service at three temperature levels for different type of end-users: The low-temperature DC (LT-DC) provides refrigeration service to, e.g., refrigerated warehouses; the medium-temperature DC (MT-DC) provides refrigeration service to commercial centers, supermarkets, etc.; and the high-temperature DC (HT-DC) that provides air-conditioning service to residential and office buildings, hotels, etc. Additionally, this subsystem of the plant operates also as a power cycle (RC-2) driven by low-grade waste heat.

- **Power cycle RC3**. This power cycle exploits the remaining low-temperature exergy of the LNG stream after going through the DC network and power cycle RC-2, since the temperature of the LNG stream at that point of the plant is still much lower than the ambient temperature. It consists of a regenerative Rankine cycle driven by the heat released from biomass combustion and using LNG as heat sink. The cycle has intermediate reheating and two expansion-stages. At present, a biomass power plant is in operation near the Barcelona LNG terminal. In many cases it is not uncommon to find availability of biomass from garden and park pruning, wood waste from construction debris and other solid waste close to urban environments.

- **Natural gas direct expansion unit (EXP)**. The LNG operating pressure in the regasification terminal is higher than that required for the NG distribution pipeline. The aim of the NG direct expansion unit is to harness the pressure exergy of NG to produce electrical power before NG is injected to the city gas distribution pipelines with the adapted pressure.

2.2 Operation of the polygeneration plant

The operation of the plant is as follows. The LNG at the exit of the boil-off-gas recondenser (stream 1) is pumped by the pump P1 up to the high pressure of the plant (7.2 MPa, stream 2). Firstly, LNG low-temperature exergy is exploited in the condenser C-1 of the power cycle RC-1. The working fluid candidates for power cycle RC-1 must have a very low freezing point to avoid crystallization in condenser C-1. The pump P2 pressurizes the working fluid which is preheated in the recuperator R-1 and superheated in the seawater heat exchanger H-1. Next, the working fluid is first expanded down to the intermediate pressure in the high-pressure turbine (T1-HP), reheated in H-1, and it is expanded again in the low-pressure turbine (T1-LP).

Afterwards, low-temperature exergy of downstream LNG at point 3 is used as heat sink of the heat transfer media of the DC network. Since power cycle RC-1 contributes to increase the temperature of LNG, the risk of crystallization of the DC heat transfer media decreases in condenser C-2. In the DC network, the pump P3 raises the pressure of the condensed heat transfer media which is also the working fluid of the power cycle RC-2. The cold distribution to the different type of end-users is made in parallel arrangement to facilitate the cold distribution and the control of the system. Therefore, all the end-users receive the cold at the same temperature (streams 24, 26, 28), regardless of their required temperature of use. The latent heat of vaporization of the heat transfer media is exploited in the end-users' substations (heat exchangers C-4, C-5 and C-6) and the secondary refrigerant used is ammonia for the facilities of the LT-DC and the MT-DC and water in the case of the HT-DC. The heat transfer media streams leaving all the end-users substations are joined in a single stream (stream 30) and superheated by low-grade waste heat (e.g., from auxiliary equipment) in the heat exchanger H-2. Next, it is expanded in the turbine T2 to produce mechanical power.

The LNG leaving condenser C-2 (stream 4) has low-temperature exergy enough to be exploited in the condenser C-3 of power cycle RC-3. The condensed working fluid (stream 45) is pumped by pump P4, preheated in the recuperator R-2 and superheated in the biomass boiler. The working fluid is first expanded in the high-pressure turbine (T3-HP). In a second expansion stage, the reheated working fluid (stream 42) is expanded in the low-pressure turbine (T3-LP). At the exit of the condenser C-3 (stream 5) and previously to exploit the NG pressure exergy, the NG is heated up to 5^{o}C using seawater.

Finally, the pressure exergy of stream 6 is exploited by the NG direct expansion unit to produce mechanical power. The expansion takes place from the operating pressure of the LNG and NG in the plant (7.2 MPa) to the set-point pressure of the city gas distribution (3 MPa). The supply temperature of the regasified NG is adjusted to the pipeline requirements in the seawater heater H-5, just before to adjust the calorific value of NG, odorize NG and feed the city gas into the distribution pipeline.

2.3 Plant modelling

The polygeneration plant with LNG physical exergy exploitation is modelled with the software Engineering Equation Solver [37]. Table 1 depicts the simulation parameters, such as temperatures, pressures or flow rates, and the modelling assumptions are listed below:

- System operation under steady-state conditions.
- Thermal and pressure losses are neglected except in the distribution pipelines of the DC network.
- Kinetic and potential energies are neglected.
- The composition of LNG is assumed as pure methane.
- Seawater is assumed as regular water.
- Saturated liquid state is supposed for working fluids and heat transfer fluid streams leaving the condensers C-1, C-2 and C-3 (streams 14, 21 and 45).
- Streams of heat transfer media in the DC network leaving the heat exchangers C-4, C-5 and C-6 are at saturated vapor state (streams 25, 27 and 29).
- Streams of secondary refrigerants are at saturated vapor state at the inlet of heat exchangers C-4 and C-5 (streams 32 and 34) and at saturated liquid state at the outlet (streams 33 and 35).
- Isentropic efficiency of turbines and NG expander: 85%.
- Isentropic efficiency of pumps: 75%.
- Mechanical losses in reduction gears and electricity losses in generators are neglected.
- A pressure of 300 kPa is assumed for seawater in heat exchangers H-1, H-4 and H-5 (streams 17-18, 48-49 and 50-51, respectively) and also for the waste heat (stream 38-39) in heat exchanger H-2.

The heat transfer in the heat exchangers of the plant is calculated from energy balance equations:

$$\dot{Q} = \dot{m}_i\left(h_{i,in} - h_{i,out}\right) = \dot{m}_j\left(h_{j,out} - h_{j,in}\right) \quad (1)$$

On the other hand, the net power produced by each subsystem of the plant is calculated as:

$$\dot{W}_{net} = \sum \dot{W}_T - \sum \dot{W}_P \quad (2)$$

To compare the performance of each subsystem of the plant with the different candidate fluids, we define the specific energy produced per tonne of LNG regasified: $\dot{W}_{net}/\dot{m}_{LNG}$, given in kWh/t-LNG. Moreover, the mass flow rate is a good indicator of the size of the system. Hence, we use another indicator defined as the ratio of the mass flow rate of working fluid required to produce a unit of energy: $\dot{m}_{WF}/\dot{W}_{net}$, given in kg/kWh.

On the other hand, the thermal efficiency of the power cycles of the plant is written as:

$$\eta_{th} = \frac{\dot{W}_{net}}{\dot{Q}_{in}} \quad (3)$$

Regarding the cold transport in the District Cooling network from the LNG regasification site to the end-user's location, the pressure loss along the supply (state point 22→23) and return (19→20) distribution pipeline is calculated as follows:

$$\frac{\Delta P}{L} = f\frac{\rho v^2}{2D} \quad (4)$$

Where f is the friction factor that is calculated using the Colebrook's equation [38]:

$$\frac{1}{\sqrt{f}} = -2 \cdot \log_{10}\left(\frac{\varepsilon/D}{3.7} + \frac{2.51}{Re \cdot \sqrt{f}}\right) \quad (5)$$

A stainless-steel pipe ASTM-A333 grade 7 [34] for low temperature service is assumed for the calculations. The temperature drops (ΔT) for both the supply and return DC pipeline is calculated from Eq. (6):

$$Q_{lim} = \frac{\Delta T}{R_{cv,i}+R_{cd,t}+R_{cd,ins}+R_{cd,soil}} \quad (6)$$

The insulation (k=0.03 W/(m·K)) thickness was determined to limit the heat gain (Q_{lim}) to 30 W/m and the thermal resistance of the soil is calculated according to ASHRAE [39] assuming a buried depth of 1.5 m and a ground temperature of 15°C.

Furthermore, exergy analysis is a helpful thermodynamic technique for analyzing the performance of a system and also for determining the most suitable operating fluids [40]. The physical exergy content due to temperature and pressure ($\dot{E}x_{ph} = \dot{E}x_T + \dot{E}x_p$) of each state point is written as:

$$\dot{E}x_{ph,i} = \dot{m}_i[(h_i - h_0) - T_0(s_i - s_0)] \quad (7)$$

The reference-environment for the exergy calculations is set to 298 K and 101.3 kPa. Particularly, the physical exergy due to temperature and pressure are calculated from Eq. (8) and (9), respectively [16]:

$$\dot{E}x_{T,i} = \dot{E}x_{ph}(T_i, p_i) - \dot{E}x_{ph}(T_0, p_i) \quad (8)$$

$$\dot{E}x_{P,i} = \dot{E}x_{ph}(T_0, p_i) - \dot{E}x_{ph}(T_0, p_0) \quad (9)$$

On the other hand, the exergy destroyed in each component of the plant is calculated as follows:

$$\dot{I} = \dot{E}x_{in} - \dot{E}x_{us} - \dot{E}x_{out} \quad (10)$$

Table A1 in Appendix A shows both the energy an exergy balances for each component of the plant.

The exergetic efficiency of each subsystem of the plant ($\eta_{ex} = \sum \dot{E}x_{us} / \sum \dot{E}x_{in}$) is expressed as:

$$\eta_{ex,RC1} = \frac{\dot{W}_{T1-HP}+\dot{W}_{T1-LP}}{(\dot{E}x_2-\dot{E}x_3)+\dot{W}_{P2}} \quad (11)$$

$$\eta_{ex,DC\&RC2} = \frac{\dot{W}_{T2}+(\dot{E}x_{33}-\dot{E}x_{32})+(\dot{E}x_{35}-\dot{E}x_{34})+(\dot{E}x_{37}-\dot{E}x_{36})}{(\dot{E}x_3-\dot{E}x_4)+\dot{W}_{P3}} \quad (12)$$

$$\eta_{ex,RC3} = \frac{\dot{W}_{T3-HP}+\dot{W}_{T3-LP}}{(\dot{E}x_4-\dot{E}x_5)+\dot{W}_{P4}} \quad (13)$$

$$\eta_{ex,EXP} = \frac{\dot{W}_{EXP}}{(\dot{E}x_5-\dot{E}x_7)+\dot{W}_{P1}} \quad (14)$$

Finally, we use a turbine size parameter [33,41,42] to account the turbines sizes, but without pretending to perform a detailed design of the turbine. This parameter is proportional to the actual turbine size and it is defined as:

$$TSF = \dot{V}_{out}{}^{1/2} \cdot \Delta h_{is}{}^{-1/4} \quad (15)$$

Where $\dot{V}_{out}$ is the volumetric flow rate at the exit of the turbine (in m^3/s) and Δh_{is} is the isentropic specific enthalpy drop in the turbine (in J/kg). The turbine size parameter and the flow rates are indicators of the relative cost of the system.

2.4 Performance indicators

To evaluate the performance of the whole plant, we define some performance indicators. These indicators are divided into two categories: (1) Thermodynamic performance indicators and (2) energy and environmental impact indicators. The thermodynamic indicators are:

- **Total net power of the plant ($\dot{W}_{net,tot}$)**. This indicator accounts for the total net power produced by each subsystem of the plant (RC-1, RC-2, RC-3 and the NG direct expansion unit):

$$\dot{W}_{net,tot} = \dot{W}_{net,RC1} + \dot{W}_{net,RC2} + \dot{W}_{net,RC3} + \dot{W}_{net,EXP} \quad (16)$$

- **District Cooling Service (DCS)**. This indicator accounts for the total refrigeration supplied by the DC network to the end-users:

$$DCS = \dot{Q}_{DC,LT} + \dot{Q}_{DC,MT} + \dot{Q}_{DC,HT} \quad (17)$$

Particularly, to compare the results obtained using the different candidate heat transfer fluids in sections 3.2, we use a specific DCS defined as the total refrigeration produced by the DC network per each tonne of LNG regasified by the plant: $DCS/\dot{m}_{LNG}$, given in kWh/t-LNG. Also, the mass flow rate of heat transfer fluid required to produce a unit of refrigeration is used as relative indicator to compare all the candidates from a homogeneous basis: $\dot{m}_{HTF}/DCS$, given in kg/kWh.

- **Equivalent Electricity Production (EEP)**. This indicator accounts for the electrical power produced and the DCS converted into electric terms by means of the Energy Efficiency Ratios (EER):

$$EEP = \dot{m}_{LNG}{}^{-1}\left(\dot{W}_{net,tot} + \frac{\dot{Q}_{DC,LT}}{EER_{ref,LT}} + \frac{\dot{Q}_{DC,MT}}{EER_{ref,MT}} + \frac{\dot{Q}_{DC,HT}}{EER_{ref,HT}}\right) \quad (18)$$

For a refrigeration system, the EER is defined as the ratio of refrigeration capacity to the total rate of electric input. The lower the set-point temperature, the lower the EER [43]. The reference EER for each temperature level of the DC network were selected according to [43] and they are: 1.3 for the LT-DC (refrigeration at -25 ^{o}C), 2.5 for the MT-DC (refrigeration at -10 ^{o}C) and 4.0 for the HT-DC (refrigeration at 5 ^{o}C).

- **Exergetic efficiency of the whole plant (η_{ex}).** It is defined as the total useful exergy output divided by the total exergy entering the polygeneration plant:

$$\eta_{ex} = \frac{\sum \dot{W}_T + \dot{W}_{EXP} + \dot{E}x_{us,DC}}{\dot{E}x_{in,LNG} + \dot{E}x_{in,WH} + \dot{Q}_{H-3}(1 - T_0/T_{bb}) + \sum \dot{W}_P} \times 100\% \quad (19)$$

Notice that the above definition produces a zero-efficiency reference case for an LNG regasification plant without exergy recovery. The exergetic efficiencies of each subsystem of the plant are also formulated following this definition pattern.

On the other hand, the energy and environmental indicators are:

- **Primary Energy Saving (PES)**:

$$PES = \eta_{ref}{}^{-1} \left(\dot{W}_{net,tot} + \frac{\dot{Q}_{DC,LT}}{EER_{ref,LT}} + \frac{\dot{Q}_{DC,MT}}{EER_{ref,MT}} + \frac{\dot{Q}_{DC,HT}}{EER_{ref,HT}} \right) \quad (20)$$

The thermal efficiency used as reference is 52% (typical combined cycle).

- **Seawater Saving (SWS)**. This indicator evaluates the seawater reduction with respect to the conventional LNG regasification process without LNG exergy recovery:

$$SWS = \left(1 - \frac{\sum \dot{m}_{SW}}{\dot{m}_{SW,ref}} \right) \times 100\% \quad (21)$$

- **Avoided carbon dioxide emissions (ACO_2e)**: This indicator estimates the amount of CO_2 emissions avoided by the polygeneration plant due to its equivalent electricity production.

$$ACO_2e = EF \left(\dot{W}_{net,tot} + \frac{\dot{Q}_{DC,LT}}{EER_{ref,LT}} + \frac{\dot{Q}_{DC,MT}}{EER_{ref,MT}} + \frac{\dot{Q}_{DC,HT}}{EER_{ref,HT}} \right) \quad (22)$$

The emissions factor (EF) represents the CO_2 emissions of a typical electricity mix integrated by diverse energy sources (e.g., natural gas, coal, nuclear energy, renewable energies, etc.). We chose an EF of 0.380 kg-CO_2/kWh as a representative value for Spain, but other values may be used depending on the reference electricity mix selected [44].

2.5 Preliminary screening of candidate fluids

A successful selection of the most suitable fluids in any energy system is essential for an appropriate performance of a system [45]. Also, the fluid selection criteria depend on the application and the environmental legislation might be a constraint [46]. The basic and common properties of the ideal fluid that may be used in any energy system and also in the subsystems of the plant presented in this paper are [47–49]:

- The *normal boiling point* (NBP) of the fluid has to be lower than the condensing temperature in order to operate above the atmospheric pressure and avoid air infiltration risk.
- The *critical temperature* of the fluid has to be higher than the design condensing temperature.
- The *freezing point* has to be low enough to avoid crystallization problems when exchanging heat with LNG.
- Large *latent heat of vaporization* to reduce the mass flow rate, reduce the size of the installation and operating cost.
- *Low viscosity* to reduce the pressure drops and thermal losses.
- *Low specific volume* (or *high density*) to reduce the energy consumption by pumping and the installation cost that are related with the size of the equipment. The volume of the fluid leaving the expander determines the turbine size.
- *Chemical stability* at the operating temperatures.
- *Safe* (nontoxic, nonflammable, noncorrosive, etc.).
- *Environmentally friendly* (null ozone depletion potential – ODP and low global warming potential – GWP).
- *Good availability* and *low cost*.

Although the characteristic listed above are the most desirable, it is difficult to find a fluid that meets all them. On the other hand, the subsystems of the polygeneration plant presented in this paper operate with lower condensing temperatures that the typical RCs [48] and with lower temperature than common District Cooling networks [50]. Therefore, the characteristics of the working fluids and heat transfer fluids that operate in this kind of plant have some particularities. For example, the candidate fluids for this plant must have much lower freezing point than most of the common fluids used in ORCs which condense at ambient temperature. Moreover, the NBP of the fluid has a particular importance in cryogenic power systems. If the condensation temperature is lower than the NBP of the fluid, the condensing pressure is below the atmospheric pressure and air infiltration may occur. Thus, the freezing of air moisture might cause problems. Also, flammable mixtures can be generated if using flammable working fluids [16].

Table 2 shows the thermophysical properties [51], global warming potential (GWP) [52] and ASHRAE safety group (flammability and toxicity) [53] of the potential candidate fluids for the polygeneration plant. The traditional classification of fluids as ‘wet’, ‘dry’ or ‘isentropic’ is not so useful in this case. For certain fluids, this classification depends on the operating conditions [54], which are significantly different for each subsystem of the polygeneration plant. On the other hand, despite some refrigerants such as R11, R12, R13, R22, R123, R115 and R502 may be also potential candidates due to their low freezing point, they are dismissed because all them are ozone depletion substances. The particular operating constraints for the candidate fluids of each subsystem of the plant are the following:

- **Power cycle RC-1**: Condensing temperature (T_{14}) = max(-130^{o}C, NBP+1^{o}C) to ensure condensation above atmospheric pressure; Freezing point < min(-100^{o}C, T_{14}) to prevent crystallization in the

condenser; and critical temperature > than condensing temperature to allow condensation in heat exchanger C-1.

- **DC and power cycle RC-2**: NBP < DC supply temperature (T_{21}=-50°C) to ensure working above atmospheric pressure; Freezing point lower than the DC supply temperature to prevent crystallization in the condenser; and critical temperature > than the design temperature at the exit of heat exchanger C-4, C-5 and C-6 ($T_{25} = T_{27} = T_{29}$ =-30°C) to allow the condensation in heat exchanger C-2.

- **Power cycle RC-3**: NBP < than the condensing temperature (T_{45}=-10°C); Limit of EoS (T_{max} in Table 2) higher than the top temperature of the cycle (T_{40} and T_{42} = 300°C). Critical temperature > than condensing temperature to allow condensation in heat exchanger C-3.

3. Results and discussion

A comparative assessment is performed between different candidate working fluids and heat transfer fluids for each subsystem of the polygeneration plant with LNG exergy recovery. The results obtained for each subsystem of the plant are presented in the following order: Power cycle RC-1 (section 3.1); District Cooling network and the power cycle RC-2 (section 3.2); and power cycle RC-3 (section 3.3). Finally, the performance of the whole polygeneration plant is evaluated when operating with the previously selected fluids (section 3.4). The candidate fluids for each subsystem of the plant are chosen according with the constraints described in section 2.5.

3.1 Fluid selection for the power cycle RC-1

To select the most suitable working fluid for the power cycle RC-1, we considered as indicators the power produced, the mass flow rate of working fluid, the seawater consumption, the size of the turbine and both the thermal and the exergetic efficiencies. Figure 2 shows the performance results for each preselected candidate fluid that fits the operating constraints stablished for the power cycle RC-1. Both the high pressure and the intermediate pressure are calculated to optimize the net power. The following observations can be made:

- Figure 2 (a) shows the power production by metric ton of LNG and the high pressure of the cycle for each candidate fluid. Since a low NBP entails a low condensation temperature (because of the condensing pressure has to be above the ambient pressure), the candidate working fluids with the lowest NBP report the highest energy production. In this sense, methane is the working fluid that reports the highest energy produced by metric ton of LNG (10 kWh/t-LNG) followed by R14 (9.6 kWh/t-LNG). Oxygen and argon also report an acceptable net power produced, although their top pressures are much higher than that for the rest of candidate fluids and this will imply a major installation cost. Thus, oxygen and argon are dismissed as working fluids for the power cycle RC-1. On the other hand, R152a and R134a give the lowest power production (< 2.5 kWh/t-LNG).

- As shown in Fig. 2 (b), methane reports the lowest mass flow rate of working fluid and seawater demand (17 kg/kWh and 0.57 t/kWh, respectively), which is economically positive. In the comparison with R14, methane requires 72% lower mass flow rate, while the seawater consumption is similar. In the case of ethylene, it reports also a low mass flow rate (22 kg/kWh) and a low seawater consumption (0.68 t/kWh). However, ethylene produces 22.7% less energy by metric ton of LNG than methane (see Fig. 2 (a)) and also the size of the turbine required is higher, which implies higher costs (see Fig. 2 (c)). On the other hand, R218 and R152a reports the highest working fluid mass flow rate and seawater demand, respectively.

- Regarding the thermal and exergetic efficiencies of the power cycle RC-1 shown in Fig. 2 (d), methane reports one of the highest values (30.2% and 35.2%, respectively). In the case of R14, despite it has a thermal efficiency of 29.5% and an exergetic efficiency of 32.4%, it is dismissed as working fluid because of its environmental impact (high GWP) and its high turbine size factor in comparison with, e.g. methane, as shown in Fig. 2 (c). Furthermore, the working fluids with relatively high NBP (propane, propylene, R32, R134a, R143a, etc.) report the lowest both thermal and exergetic efficiencies, so they are not suitable for LNG exergy recovery in the power cycle RC-1.

Fig. 2. Performance results for each candidate working fluid in the power cycle RC-1. (a) Specific energy and high pressure. (b) Required mass flow rate of working fluid to produce a unit of energy and seawater consumption. (c) Turbine size factor for the turbines T1 (HP) and T1 (LP). (d) Thermal and exergetic efficiencies. Shaded area represents the desired performance.

According to the results, methane is selected as the working fluid for the power cycle RC-1. Despite its flammability risk, methane is a natural fluid and it shows the best trade-off between all the performance indicators taken into account in the selection of working fluid for the power cycle RC-1.

3.2 Fluid selection for the District Cooling network and the power cycle RC-2

The transport of the cold from the LNG regasification site to the end-users is a critical constraint in the DC network and the power cycle RC-2. As shown in Fig. 1, unlike the other subsystems of the polygeneration plant that only produce mechanical power (power cycle RC-1, power cycle RC-3 and NG direct expansion unit), in the DC network and the power cycle RC-2 the length of pipelines is in the order of kilometers. Thus, depending on the heat transfer fluid selected the pressure drop and heat loss due to transport affects the performance significantly. Although the priority of this subsystem of the plant is to provide refrigeration service, the power production is also analyzed. Fluid flow rates, thermal and exergetic efficiencies, turbine size factors and pipeline characteristics are evaluated and compared. Figure 3 and Table 3 shows the performance results for each candidate fluid in the combined DC network and power cycle RC-2. The following observations can be made:

- Figure 3 (a) shows the refrigeration service provided to the end-users and the required mass flow rate of heat transfer fluid for each candidate fluid. R32 provides the highest DCS (95.1 kWh/t-LNG) followed by R41 (91.7 kWh/t-LNG). By the other side, R41 is the fluid which requires the lowest mass flow rate to provide a unit of cooling (8 kg/kWh). Although R410A reports an acceptable performance, it is dismissed because its high GWP and its lower refrigeration service compared with R32 (which is being used as substitute of R410A in refrigeration systems [55]). Besides, CO_2 exhibits a good performance, with a DCS of 90.8 kWh/t-LNG (higher than the obtained with ethane, ethylene and R23, but 4% lower than the given by R32) and a required mass flow rate of 10.5 kg/kWh. It is also remarkable that R116 reports both the lowest refrigeration service and the highest mass flow rate. This is mainly because of its low latent heat of vaporization (see Table 3).

- Figure 3 (b) shows the power produced by metric to of LNG and the fluid mass flow rate required to produce a unit of power. R41 is the candidate with the highest energy production (6.8 kWh/t-LNG) and the lowest mass flow rate required to produce a unit of power (109 kg/kWh). The power production of R32 is 3 % lower than that for R41 and the required mass flow rate to produce a unit of power is 23.8% higher than that for R41. Although ethane achieves 3.6% higher power output than CO_2 and a lower mass flow rate than CO_2, these differences are not higher enough to justify the higher both environmental impact and the safety risk of ethane with respect to CO_2. Also, Fig. 3 (c) shows that the turbine size factor and the waste heat demand when using CO_2 are lower than that for ethane. Thus, ethane is dismissed as candidate fluid for the DC network and the power cycle RC-2. On the other hand, since ethylene and R23 both have a lackluster performance not only in the power production, but also in the refrigeration service, they are dismissed as candidate fluids.

- Figure 3 (d) shows the thermal efficiency and the exergetic efficiency of the DC network and the power cycle RC-2 for the candidate working fluids. Altogether, the values of thermal efficiencies obtained are quite poor (<6.2%). This is because the subsystem DC + RC-2 is not designed to produce power exclusively, but the priority is the refrigeration service. As a consequence, the pressures of the cycle are not optimized for power production, but are constrained by the refrigeration set-point temperatures. While R41 has the highest thermal efficiency (6.2%), R32 has the highest exergetic efficiency (31.1%). Anyway, the differences in the thermal and exergetic efficiencies between R32 and R41 are very small. On the other hand, CO_2 has higher exergetic efficiency than ethane, but a lower thermal efficiency.

- Because of its high liquid and vapor density CO_2 is one of the fluids with the smallest pipelines section for both the supply and return pipelines (see Table 3). This fact is positive from the economical point of view. In the case of R32, it has a low-section supply pipeline due to its high liquid density, but it has the largest section of the return pipeline because of it has the lowest vapor density among the candidate fluids. R41 requires pipelines with larger section than CO_2 but lower than R32. On the other hand, since R41 is one of the candidate fluids with the lowest viscosity, it reports a low pressure drop in comparison with the rest of fluids and that means a lower pumping consumption to overcome the pressure losses. Furthermore, the price of the fluid has to be taken into account due to

the large distance of the pipeline network, which implies large volume of fluid. In this sense, CO_2 is very competitive because it is a naturally abundant fluid.

Fig. 3. Performance analysis of the DC network and the power cycle RC-2 for each candidate fluid: (a) Power produced and high pressure of the cycle. (b) Working fluid mass flow rate required per unit of energy produced. (c) Turbine T2 size indicator and waste heat (water) demand. (d) Thermal and exergetic efficiencies. Shaded area represents the desired performance.

Once the results have been analyzed we can summarize that: R32 achieves the highest refrigeration service and exergetic efficiency; R41 achieves the highest power production and thermal efficiency, and the lowest mass flow rate required to produce a unit of refrigeration and a unit of power. However, CO_2 has a notable balance between all the criteria with a performance relative similar to R-32 and R-41. Moreover, CO_2 is a natural fluid with a lower environmental impact and a more competitive cost. Therefore, CO_2 is selected as working media for the DC network and power cycle RC-2.

3.3 Fluid selection for the power cycle RC-3

The power cycle RC-3 operates with a high temperature similar to common ORCs driven by biomass combustion heat (300 ^{o}C) [48], but with a much lower condensation temperature (-10 ^{o}C), so that typical working fluids used for ORCs in biomass power plants (e.g., toluene or ethylbenzene [56]) are out of selection. Also, the limited temperature range for equation of state (EoS) of some potential candidate fluids it is a constraint for the working fluid selection process [51]. Apart from the candidate preselected from Table 2 that satisfy the constraint for power cycle RC-3, we also consider the binary zeotropic mixture ammonia-water (with ammonia mass fractions of 70% and 90%) as candidate because it is widely investigated for LNG exergy recovery systems [57–59]. The high and intermediate pressures of the cycle are optimized from thermodynamic point of view to maximize the power produced. Therefore, the calculated pressures might stablish a benchmark for a future engineering stage in which the expander will be selected. All the candidate fluids are compared with respect to the power produced, the working fluid mass flow rate required, the turbine size and the thermal and exergetic efficiencies. Figure 4 shows the performance results obtained by each candidate working fluid in the power cycle RC-3. The following observations can be made:

- Figure 4 (a) shows the energy production by metric ton of LNG and the high pressure of the cycle for each candidate fluid. According to the results, propane is the candidate that is able to produce the highest specific energy (41.8 kWh/t-LNG) with one of the lowest top-pressure of the cycle. Also, propylene achieves a large energy production (41.1 kWh/t-LNG), although with a slightly higher pressure than propane. On the other hand, the pair ammonia-water (90% NH_3) reports a 5% higher power production than pure ammonia, and 9.4% higher than the pair ammonia-water (70% NH_3). Besides, the optimal high-pressure for ammonia-water pair (90% NH_3) is the lowest among all the

candidates, so that it may result in lower installation costs. On the contrary, CO_2 reports one of the lowest energy production (35 kWh/t-LNG) and it requires the highest pressure for optimizing the power produced, which has a negative impact on costs.

- Figure 4 (b) shows the mass flow rate of working fluid required to produce a unit of energy and the specific heat recovered in the recuperator R-2. The results show that pure ammonia and ammonia-water pairs (70% and 90% NH_3) need the lowest mass flow rates to produce a unit of energy (around 5 kg/kWh), which has positive impact on costs. In contrast, CO_2 and R143a require the highest mass flow rates (23 and 27 kg/kWh, respectively), so both are dismissed as candidates. On the other hand, propane requires 13.6 kg/kWh, which is lower than that for propylene and ethane. Regarding the recuperator, ammonia-water pair (90% NH_3) has the best specific heat recovering (131 W/kg), followed by ethane and propane. Ammonia recovers only 62 W/kg. To understand these results, Fig. 5 illustrates the profile of temperatures in the recuperator for propane, ammonia and ammonia-water (90% NH_3). As it can be seen, the temperatures of hot and cold stream for the ammonia-water (90% NH_3) approach better each other along the recuperator. This fact is also positive for the reduction of irreversibilities.

- Concerning the turbine size, Fig. 4 (c) shows the turbine T3 size factor (both T3-HP and T3-LP). CO_2, ethane, ammonia and ammonia-water pair (70% NH_3) require the lowest sizes, which may involve lower costs [41,60]. Propane, propylene and R134a require the higher sizes mainly due to their larger specific volumes after the expansion. Figure 4 (d) shows the thermal and the exergetic efficiencies obtained. Ethane is the fluid that achieves the highest exergetic efficiency: 45.1%. However, this value is not higher enough than the given by propane (44.4%) to outweigh the lower power production and the higher pressure required by ethane. Moreover, propane is the fluid with the highest thermal efficiency: 37.8%. Despite propylene also shows high efficiencies, they are lower than that for propane and its environmental impact and security issues are unimproved, so propylene is dismissed as working fluid. Moreover, ammonia and ammonia-water pairs, together with CO_2, show the poorest values of efficiencies.

Fig. 4. Performance analysis of the power cycle RC-3 for each candidate fluid: (a) Power produced and high pressure of the cycle. (b) Working fluid mass flow rate required per unit of energy produced. (c) Turbine size factor for T3 (HP) and T3 (LP). (d) Thermal and exergetic efficiencies. Shaded area represents the desired performance.

Fig. 5. Temperature profile in the recuperator R-2 of the power cycle RC-3 for propane, ammonia and ammonia-water pair (ammonia mass fraction 90%) as working fluids.

According to the results and despite neither of the simulated fluids achieves all the desirable properties, propane is selected as working fluid for the power cycle RC-3 because of it shows the best trade-off between all the selection criteria. Although propane is a natural fluid with a low GWP, its flammability risk must be considered and precautions have to be taken in a further design of the plant.

3.4 Performance of the whole polygeneration plant

Once the fluid selection is completed for each subsystem of the polygeneration plant, we evaluate the performance of the whole plant. Table 4 shows a comparison of the performance of the typical LNG regasification process (that uses seawater as heat source without cold utilization) and the performance of the polygeneration plant that we propose in this paper. In addition, this table is a breakdown of the contribution of each subsystem of the total performance of the plant. According to the results, the following observations can be made:

- If LNG physical exergy is wasted as in the typical LNG regasification process, the plant consumes 1.1 MW of electricity (LNG pumping). Besides, no mechanical power is produced and the LNG physical exergy is wasted. On the other hand, the proposed polygeneration plant with exergy recovery from LNG-regasification produces a mechanical power of 73.3 kWh/t-LNG (13.2 MW). For instance, this is 83% higher than the specific power produced by the cryogenic power plant nº2 of Osaka Gas in Senboku II terminal (40 kWh/t-LNG) [35]. On the other hand, the power cycle RC-3 is the one which contributes the most to the total power production of the plant (57%), while the electric power given by the DC network and power cycle RC-2 is the lowest (7.6%).

- The DC network provides 16.4 MW of refrigeration service (91.1 kWh/t-LNG) to the end-users, distributed for each temperature level as follows: 8.2 MW for the low-temperature for the low-temperature network; 6.6 MW for the medium-temperature network; and 1.6 MW for the high-temperature network. To account for both the electricity production and the refrigeration service simultaneously in a single indicator, the Equivalent Electricity Production (Eq. (18)) is used. According with this combined parameter, the polygeneration plant achieves an equivalent electricity production of 125.3 kWh from each metric ton of LNG regasified. Therefore, the plant can recover more than 15% of the electric energy consumed by the compressors of the refrigeration systems in a typical LNG liquefaction plant (805 kWh/t-LNG produced [61]).

- Regarding the environmental impact, the proposed polygeneration plant reduces by 60% the amount of seawater utilized in a common LNG regasification plant. Also, it reports an annual primary energy saving of 380 GWh and it avoids the annual emission of 75,079 tons of CO_2 to the atmosphere (47.6 kg-CO_2/t-LNG). Moreover, all the selected fluids for the plant are natural fluids with low GWP, so the environmental impact is negligible if a leakage of fluids in the installation occurs.

Table A2 in Appendix A shows the main thermodynamic data of each state point of the polygeneration plan illustrated in Fig. 1 operating with the selected fluids.

Furthermore, to perform an exergy analysis is convenient and instructive in LNG exergy recovery systems. Figure 6 depicts how LNG physical exergy is exploited by each subsystem of the plant. The two components of the LNG physical exergy (pressure exergy and low-temperature exergy) are identified in this diagram. A remarkable fact is that the maximum LNG physical exergy that can be exploited by the plant is limited to 53% of the total LNG physical exergy content at the exit of pump P-1. This is because the temperature and pressure of the regasified natural gas are constrained by the city gas distribution pipeline (5 ^{o}C and 3 MPa, respectively). Thus, the still remaining low-temperature and pressure components of LNG exergy at the exit of the heat exchanger H-5 cannot be exploited by the plant.

Fig. 6. Detailed exergy flow chart of the LNG physical exergy utilization (temperature exergy + pressure exergy) in the proposed polygeneration plant. Nomenclature: PE – Pressure exergy; LTE – Low-temperature exergy.

The power cycle RC-1, the DC network and the power cycle RC-2 and the power cycle RC-3 only exploit the low-temperature exergy of LNG. On the other hand, the NG direct expansion unit exploits the LNG pressure exergy available between 7.2 MPa and 3 MPa. Although most of the low-temperature exergy is exploited by the DC network and more than 90 kWh/t-LNG of refrigeration are supplied to the end-users, the useful exergy harnessed by the DC network is low: Only 9% of the total LNG physical exergy exploited by the plant. This is because of the relative high temperature (from the exergetic point of view) required by the end-users. By decreasing the supply temperature of the DC network and also the temperature required by the end-users, the exergetic efficiency of the DC network will increase.

Finally, Fig. 7 shows an exergy flow chart of the whole LNG supply chain. The aim of this figure is to offer the reader a broad view about how the proposed polygeneration plant is integrated in the whole LNG value chain. The exergy path represented in this figure is described as follows. After extraction and before liquefaction, the raw gas has only chemical exergy. However, once liquefied (the liquefaction facility consumes approximately 10% of the total gas processed as fuel [62]) the LNG gets also physical exergy because of its low temperature. Afterwards, part of the LNG transported in LNG carriers is consumed as fuel. In the receiving terminals, the LNG from tanks is pressurized before its regasification in the polygeneration plant, so the pressure exergy of LNG increases. Although it is remarkable that the physical exergy of LNG due to its low-temperature and pressure represents only around 2% of the total exergy content of NG, this value must not be misunderstood. This value seems to be very low because of the high chemical exergy content of NG as fuel but the physical exergy of LNG is not negligible and it can be recovered in multiple industrial applications.

Fig. 7. Exergy flow chart of natural gas supply chain with the integration of the proposed polygeneration plant with exergy recovery from LNG-regasification. The 100-base is assumed as the chemical exergy as fuel of 1 metric ton of natural gas.

As shown in Fig. 7, the polygeneration system proposed in this paper exploits only the physical exergy of LNG and the regasified natural gas supplied to the end-users (city gas) preserves all its chemical exergy as fuel. According to the results and the definition given by Eq. (19), the exergetic efficiency of the proposed polygeneration plant is 40.6%, which is nearly double than the achieved by actual cryogenic power systems [27].

4. Conclusions

In this paper, we dealt with the selection of fluids and the performance analysis of a polygeneration plant with LNG exergy recovery. A comparative assessment is performed between different candidate working fluids and heat transfer fluids for each subsystem of the plant by using thermodynamic and environmental indicators. Once the fluids are selected, we evaluate the performance of the whole plant. The main conclusions are:

1. All the selected fluids have some weaknesses and although neither of the candidate fluids is the best for all the performance indicators, we have selected the fluids that achieve the best trade-off between all the indicators: Methane for the power cycle RC-1; Carbon dioxide for the DC network and the power cycle RC-2; and propane for the power cycle RC-3. It is remarkable that all the selected fluids are natural fluids. Also, the secondary fluids of the DC network are natural fluids (ammonia and water).

2. The polygeneration plant produces 73.3 kWh/t-LNG of net electrical energy and 91 kWh/t-LNG for refrigeration. Also, the plant reports an equivalent electricity production of 125.3 kWh/t-LNG and avoid the annual emission of more than 75,000 tons of CO_2 to the atmosphere. Moreover, the plant reduces the seawater consumption up to 60% with respect to the typical LNG regasification process without exergy recovery.

3. The exergetic efficiency of the polygeneration plant is 40.6%. From the total exergy input in the plant, 35% is converted into electricity and 9% of the LNG exergy is harnessed for refrigeration. Furthermore, the proposed polygeneration plant recovers 15% of the electrical energy consumed by the refrigeration systems utilized for the liquefaction of natural gas in conventional liquefaction facilities.

Acknowledgements

Antonio Atienza-Márquez acknowledges the Spanish Ministry of Education, Culture and Sport (MECD) the financial support of the predoctoral contract FPU15/04514.

Appendix A

Table A1 of this appendix shows the energy and exergy balances of each component of the polygeneration plant. On the other hand, Table A2 shows the main thermodynamic data of each state point of the polygeneration plant analyzed in this paper operating with the selected working fluids and heat transfer fluids.

References

[1] International Institute of Refrigeration (IIR), Kyoto Protocol, 2017.

[2] BP p.l.c., BP Energy Outlook 2018 Edition, (2018) 125. https://www.bp.com/en/global/corporate/energy-economics/energy-outlook.html (accessed May 7, 2018).

[3] International Energy Agency (IEA), CO2 Emissions from Fuel Combustion 2017, OECD Publishing, Paris, 2017. doi:10.1787/co2_fuel-2017-en.

[4] J.C. Peters, Natural gas and spillover from the US Clean Power Plan into the Paris Agreement, Energy Policy. 106 (2017) 41–47. doi:10.1016/j.enpol.2017.03.039.

[5] International Gas Union (IGU), The natural gas industry: Methane emissions challenge, (2017) 23.

[6] S. Kumar, H.-T. Kwon, K.-H. Choi, W. Lim, J.H. Cho, K. Tak, I. Moon, LNG: An eco-friendly cryogenic fuel for sustainable development, Appl. Energy. 88 (2011) 4264–4273. doi:10.1016/j.apenergy.2011.06.035.

[7] Royal Dutch Shell plc, LNG Outlook, 2017. https://www.shell.com/energy-and-innovation/natural-gas/liquefied-natural-gas-lng/lng-outlook.html (accessed November 25, 2017).

[8] BP plc, BP Energy Outlook, 2017. https://www.bp.com/content/dam/bp/pdf/energy-economics/energy-outlook-2017/bp-energy-outlook-2017.pdf (accessed September 13, 2017).

[9] International Gas Union (IGU), 2018 World LNG Report, 27th World Gas Conference Edition, 2018.

[10] B.B. Kanbur, L. Xiang, S. Dubey, F.H. Choo, F. Duan, Cold utilization systems of LNG: A

review, Renew. Sustain. Energy Rev. 79 (2017) 1171–1188. doi:10.1016/j.rser.2017.05.161.

[11] R. Ferreiro García, J. Jose, Carbia Carril, J. Romero Gómez, M. Romero Gómez, Combined cascaded Rankine and direct expander based power units using LNG (liquefied natural gas) cold as heat sink in LNG regasification, Energy. 105 (2016) 16–24. doi:10.1016/j.energy.2015.09.051.

[12] A. Ebrahimi, M. Ziabasharhagh, Optimal design and integration of a cryogenic Air Separation Unit (ASU) with Liquefied Natural Gas (LNG) as heat sink, thermodynamic and economic analyses, Energy. 126 (2017) 868–885. doi:10.1016/j.energy.2017.02.145.

[13] Y. Li, H. Luo, Integration of light hydrocarbons cryogenic separation process in refinery based on LNG cold energy utilization, Chem. Eng. Res. Des. 93 (2015) 632–639. doi:10.1016/j.cherd.2014.04.009.

[14] L. Zhao, H. Dong, J. Tang, J. Cai, Cold energy utilization of liquefied natural gas for capturing carbon dioxide in the flue gas from the magnesite processing industry, Energy. 105 (2016) 45–56. doi:10.1016/j.energy.2015.08.110.

[15] J. Chang, J. Zuo, K.-J. Lu, T.-S. Chung, Freeze desalination of seawater using LNG cold energy, Water Res. 102 (2016) 282–293. doi:10.1016/j.watres.2016.06.046.

[16] M. Romero Gómez, R. Ferreiro Garcia, J. Romero Gómez, J. Carbia Carril, Review of thermal cycles exploiting the exergy of liquefied natural gas in the regasification process, Renew. Sustain. Energy Rev. 38 (2014) 781–795. doi:10.1016/j.rser.2014.07.029.

[17] K. Wang, S. Dubey, F.H. Choo, F. Duan, Thermoacoustic Stirling power generation from LNG cold energy and low-temperature waste heat, Energy. 127 (2017) 280–290. doi:10.1016/j.energy.2017.03.124.

[18] T. Sung, K.C. Kim, LNG Cold Energy Utilization Technology, in: X. Zhang, I. Dincer (Eds.), Energy Solut. to Combat Glob. Warm. Notes Energy, vol. 33, Springer, 2017: pp. 47–66. doi:10.1007/978-3-319-26950-4_3.

[19] T. Otsuka, Evolution of an LNG Terminal: Senboku Terminal of Osaka Gas, in: 23rd World Gas Conf., Amsterdam (Netherlands), 2006: p. 14.

[20] S. Hirakawa, K. Kosugi, Utilization of LNG cold, Int. J. Refrig. 4 (1981) 17–21. doi:10.1016/0140-7007(81)90076-1.

[21] V. La Rocca, Cold recovery during regasification of LNG part one: Cold utilization far from the regasification facility, Energy. 35 (2010) 2049–2058. doi:10.1016/j.energy.2010.01.022.

[22] V. La Rocca, Cold recovery during regasification of LNG part two: Applications in an Agro Food Industry and a Hypermarket, Energy. 36 (2011) 4897–4908. doi:10.1016/j.energy.2011.05.034.

[23] S. Li, B. Wang, J. Dong, Y. Jiang, Thermodynamic analysis on the process of regasification of LNG and its application in the cold warehouse, Therm. Sci. Eng. Prog. 4 (2017) 1–10. doi:10.1016/j.tsep.2017.08.001.

[24] European Commission, European Strategic Energy Technology Plan (SET-Plan), (2017) 13. https://setis.ec.europa.eu/system/files/integrated_setplan/%0Aissues_paper_action6_ee_industry_0.pdf (accessed June 10, 2018).

[25] G. Li, Y. Hwang, R. Radermacher, Cold Thermal Energy Storage Materials and Applications Toward Sustainability, in: X. Zhang, I. Dincer (Eds.), Energy Solut. to Combat Glob. Warm. Notes Energy, vol. 33, Springer, 2017: pp. 67–117. doi:10.1007/978-3-319-26950-4_4.

[26] T. He, Z.R. Chong, J. Zheng, Y. Ju, P. Linga, LNG cold energy utilization: Prospects and challenges, Energy. 170 (2019) 557–568. doi:10.1016/j.energy.2018.12.170.

[27] R. Agarwal, Y. Hisazumi, A. Kegasa, T. Hori, Hampson type heat-exchanger technology and economic evaluation for LNG re- gasification and power generation At LNG receiving terminals, in: Proc. Int. Conf. Power Eng., The Japan Society of Mechanical Engineers, Yokohama (Japan), 2015.

[28] A. Rong, R. Lahdelma, Role of polygeneration in sustainable energy system development challenges and opportunities from optimization viewpoints, Renew. Sustain. Energy Rev. 53 (2015) 363–372. doi:10.1016/j.rser.2015.08.060.

[29] S. Murugan, B. Horák, Tri and polygeneration systems - A review, Renew. Sustain. Energy Rev. 60 (2016) 1032–1051. doi:10.1016/j.rser.2016.01.127.

[30] A. Atienza-Márquez, J.C. Bruno, A. Coronas, Cold recovery from LNG-regasification for polygeneration applications, Appl. Therm. Eng. 132 (2018) 463–478. doi:10.1016/j.applthermaleng.2017.12.073.

[31] M.H. Taheri, A.H. Mosaffa, L.G. Farshi, Energy, exergy and economic assessments of a novel integrated biomass based multigeneration energy system with hydrogen production and LNG regasification cycle, Energy. 125 (2017) 162–177. doi:10.1016/j.energy.2017.02.124.

[32] W.J. Rao, L.J. Zhao, C. Liu, M.G. Zhang, A combined cycle utilizing LNG and low-temperature solar energy, Appl. Therm. Eng. 60 (2013) 51–60. doi:10.1016/j.applthermaleng.2013.06.043.

[33] M. Badami, J.C. Bruno, A. Coronas, G. Fambri, Analysis of different combined cycles and working fluids for LNG exergy recovery during regasification, Energy. 159 (2018) 373–384. doi:10.1016/j.energy.2018.06.100.

[34] D. Pineda Quijano, C. Infante Ferreira, W. Duivenvoorden, J. Mieog, T. Van Der Noortgaete, B. Van Der Velpen, Techno-economic feasibility study of a system for the transfer of refrigeration

capacity from LNG regasification plants to industrial assets, in: 12th IEA Heat Pump Conf., Rotterdam, 2017.

[35] Osaka Gas Co. Ltd., Cryogenic power generation system recovering LNG's cryogenic energy and generating power for energy and CO2 emission savings, (2017). https://www.osakagas.co.jp/en/rd/technical/1198907_6995.html (accessed June 6, 2018).

[36] M. Tada, A supercritical pressure cold energy utilization system of the cryogenic fluid (Liquefied gas supercritical pressure cold energy power generation system : LSG), Trans. JSME (in Japanese). 82 (2016) 15-00581-15-00581. doi:10.1299/transjsme.15-00581.

[37] F-Chart Software, Engineering Equation Solver (EES), (2017). http://www.fchart.com/ees/ (Accesed 02.10.2017).

[38] Y.A. Çengel, J.M. Cimbala, Mecánica de fluidos : fundamentos y aplicaciones, McGraw Hill, México DF, 2006.

[39] ASHRAE, District heating and cooling, in: ASHRAE Handb. Heating, Vent. Air-Conditioning Syst., 2008.

[40] H. Arat, O. Arslan, Exergoeconomic analysis of district heating system boosted by the geothermal heat pump, Energy. 119 (2017) 1159–1170. doi:10.1016/j.energy.2016.11.073.

[41] A.A. Lakew, O. Bolland, Working fluids for low-temperature heat source, Appl. Therm. Eng. 30 (2010) 1262–1268. doi:10.1016/j.applthermaleng.2010.02.009.

[42] J. Bao, L. Zhao, A review of working fluid and expander selections for organic Rankine cycle, Renew. Sustain. Energy Rev. 24 (2013) 325–342. doi:10.1016/j.rser.2013.03.040.

[43] ASHRAE, ASHRAE Handbook-Refrigeration - SI Edition, 2014.

[44] B. Koffi, A. Cerutti, M. Duerr, A. Iancu, A. Kona, G. Janssens-Maenhout, CoM Default Emission Factors for the Member States of the European Union - Version 2017, European Comission, Joint Research Centre (JRC), 2017. http://data.europa.eu/89h/jrc-com-ef-comw-ef-2017 (Accesed February 2, 2019).

[45] G. Li, Organic Rankine cycle performance evaluation and thermoeconomic assessment with various applications part I: Energy and exergy performance evaluation, Renew. Sustain. Energy Rev. 53 (2016) 477–499. doi:10.1016/j.rser.2015.08.066.

[46] G. Li, M. Eisele, H. Lee, Y. Hwang, R. Radermacher, Experimental investigation of energy and exergy performance of secondary loop automotive air-conditioning systems using low-GWP (global warming potential) refrigerants, Energy. 68 (2014) 819–831. doi:10.1016/j.energy.2014.01.018.

[47] J. Bao, L. Zhao, A review of working fluid and expander selections for organic Rankine cycle, Renew. Sustain. Energy Rev. 24 (2013) 325–342. doi:10.1016/j.rser.2013.03.040.

[48] S. Quoilin, M. Van Den Broek, S. Declaye, P. Dewallef, V. Lemort, Techno-economic survey of Organic Rankine Cycle (ORC) systems, Renew. Sustain. Energy Rev. 22 (2013) 168–186. doi:10.1016/j.rser.2013.01.028.

[49] A.I. Papadopoulos, M. Stijepovic, P. Linke, On the systematic design and selection of optimal working fluids for Organic Rankine Cycles, Appl. Therm. Eng. 30 (2009) 760–769. doi:10.1016/j.applthermaleng.2009.12.006.

[50] W. Gang, S. Wang, F. Xiao, D. Gao, District cooling systems: Technology integration, system optimization, challenges and opportunities for applications, Renew. Sustain. Energy Rev. 53 (2016) 253–264. doi:10.1016/j.rser.2015.08.051.

[51] NIST, REFPROP 9.1, (2018). https://www.nist.gov/srd/refprop (accessed January 24, 2018).

[52] J.M. Calm, G.C. Hourahan, Property, safety, and environmental data for alternative refrigerants, Refrig. Sustain. Dev. Proc. 23rd Int. Congr. Refrig. (2011) Paper 915.

[53] ANSI/ASHRAE Standard 34, Designation and Safety Classification of Refrigerants, (2016).

[54] A. Groniewsky, G. Györke, A.R. Imre, Description of wet-to-dry transition in model ORC working fluids, Appl. Therm. Eng. 125 (2017) 963–971. doi:10.1016/j.applthermaleng.2017.07.074.

[55] X. Xu, Y. Hwang, R. Radermacher, Performance comparison of R410A and R32 in vapor injection cycles, Int. J. Refrig. 36 (2013) 892–903. doi:10.1016/j.ijrefrig.2012.12.010.

[56] U. Drescher, D. Brüggemann, Fluid selection for the Organic Rankine Cycle (ORC) in biomass power and heat plants, Appl. Therm. Eng. 27 (2007) 223–228. doi:10.1016/j.applthermaleng.2006.04.024.

[57] K.H. Kim, K.C. Kim, Thermodynamic performance analysis of a combined power cycle using low grade heat source and LNG cold energy, Appl. Therm. Eng. 70 (2014) 50–60. doi:10.1016/j.applthermaleng.2014.04.064.

[58] H. Habibi, A. Chitsaz, K. Javaherdeh, M. Zoghi, M. Ayazpour, Thermo-economic analysis and optimization of a solar-driven ammonia-water regenerative Rankine cycle and LNG cold energy, Energy. 149 (2018) 147–160. doi:10.1016/j.energy.2018.01.157.

[59] T. Miyazaki, Y.. Kang, A. Akisawa, T. Kashiwagi, A combined power cycle using refuse incineration and LNG cold energy, Energy. 25 (2000) 639–655. doi:10.1016/S0360-5442(00)00002-5.

[60] B. Fankam Tchanche, G. Papadakis, G. Lambrinos, A. Frangoudakis, Fluid selection for a low-temperature solar organic Rankine cycle, Appl. Therm. Eng. 29 (2008) 2468–2476. doi:10.1016/j.applthermaleng.2008.12.025.

[61] S. Le, J.-Y. Lee, C.-L. Chen, Waste cold energy recovery from liquefied natural gas (LNG) regasification including pressure and thermal energy, Energy. 152 (2018) 770–787. doi:10.1016/j.energy.2018.03.076.

[62] Total, Grow in LNG, an Energy for the Future, (2018). https://www.ep.total.com/en/areas/liquefied-natural-gas/grow-lng-energy-future (accessed July 17, 2018).

Nomenclature

Abbreviatures

1, 2, … ,51	Thermodynamic state points
ACO_2e	Avoided carbon dioxide emissions
BB	Biomass boiler
C-1…C-6	Condensers
DC	District Cooling network
DCS	District Cooling Service
EEP	Equivalent Electricity Production
EER	Energy Efficiency Ratio
EF	CO_2 Emissions factor
EoS	Equation of state
EXP	NG direct expansion unit
GWP	Global Warming Potential
H-1…H-5	Heaters
HP	High pressure
HT	High-temperature (District Cooling)
LNG	Liquefied Natural Gas
LP	Low pressure
LT	Low-temperature (District Cooling)
LTE	Low-temperature component of physical exergy
MT	Medium-temperature (District Cooling)
NBP	Normal boiling point
NG	Natural Gas
ODP	Ozone Depletion Potential
P1…P4	Pumps
PE	Pressure component of physical exergy
PES	Primary Energy Saving
R-1, R-2	Recuperators
RC	Rankine cycle

SW	Seawater
SWS	Seawater Saving
T1…T4	Turbines
TSF	Turbine/expander size parameter
WH	Waste heat

Variables

D	Diameter (m)
$\dot{E}x$	Exergy (kW)
f	Friction factor
h	Enthalpy (kJ/kg)
$\dot{I}$	Irreversibility (kW)
k	Thermal conductivity (W/(m·K))
L	Length of the main District Cooling network pipeline
$\dot{m}$	Mass flow rate (kg/s)
p	Pressure (bar)
$\dot{Q}$	Heat flux (kW)
R	Thermal resistance (m K/W)
Re	Reynold's number
s	Entropy (kJ/(kg·K))
T	Temperature (K)
v	Velocity (m/s)
$\dot{V}$	Volumetric flow rate (m^3/s)
$\dot{W}$	Power (kW)

Greek letters

Δ	Temperature or pressure drop
ε	Roughness (m)
μ	Dynamic viscosity (Pa·s)
η	Efficiency
ρ	Density (kg/m^3)

Subscripts

0	Reference environment (exergy)
bb	Biomass boiler
c	Critical point
cd	Conductive
cv	Convective
ex	Exergetic
fr	Freezing point
i	Inner
in	Entering the system
ins	insulation
is	Isentropic

lim	Limit (heat gain)
net	Net (power)
out	Leaving the system
ph	Physical (exergy)
ref	Reference
sw	Seawater
t	Tube wall
th	Thermal
us	Useful (Exergy)

Table 1. Base case operation parameters.

Subsystem of the plant	Parameter	Value
LNG	LNG mass flow rate, ($\dot{m}_{LNG}$)	180 t/h
	LNG storage pressure, (p_1)	0.13 MPa
	LNG storage temperature, (T_1)	-162^{o}C
	Operating pressure of LNG in the plant	7.2 MPa
	Temperature at the exit of C-1, C-2 and C-3 (T_3, T_4, T_5)	-135/-65/-15^{o}C
Power cycle RC-1	Minimum condensing temperature RC-1	-130^{o}C
	Inlet temperature of turbine T1 (HP) and T1 (LP), (T_9, T_{11})	10^{o}C
	Pinch temperature difference in recuperator R-1	10^{o}C
	Seawater inlet/outlet temperature H-1	20/15^{o}C
DC + power cycle RC-2	DC share of refrigeration demand LT/MT/HT	50/40/10%
	Temperature at the exit of C-4, C-5 and C-6 (T_{25}, T_{27}, T_{29})	-30^{o}C
	DC supply temperature (main pipeline)	-50^{o}C
	Length of DC supply (points 22→23) and return (points 19→20) pipelines	2 km
	Secondary fluid (water) supply/return temperature HT-DC	5/12^{o}C
	Secondary refrigerant (ammonia) supply temperatures LT/MT	-25/-10^{o}C
	Inlet temperature of turbine T2, (T_{31})	30^{o}C
	Waste heat (water) stream inlet/outlet temperature, (T_{38}, T_{39})	40/35^{o}C
Power cycle RC-3	Combustion temperature inside biomass boiler, (T_{bb})	850^{o}C
	Condensing temperature RC-3	-10^{o}C
	Pinch temperature difference in recuperator R-2	15^{o}C
	Inlet temperature of turbine T3 (HP) and T3 (LP), (T_{40}, T_{42})	300^{o}C
NG direct expansion unit	Inlet temperature of EXP, (T_6)	5^{o}C
	Seawater inlet/outlet temperature H-4, H-5	20/15^{o}C
	Temp. of NG supplied to distribution pipeline, (T_8)	5^{o}C
	Pressure of NG supplied to distribution pipeline, (p_8)	3 MPa

Table 2. Thermophysical properties, environmental data and safety group of candidate fluids.

Fluid	Type	T_{fr}, °C	NBP, °C	T_c, °C	P_c, kPa	T_{max} [a], °C	GWP [b]	Safety group [c]
R732 (Oxygen)	I.C.	-218.79	-182.96	-118.57	5,043	1726.85	-	n.d.
R740 (Argon)	I.C.	-189.34	-185.85	-122.46	4,863	1726.85	-	A1
R290 (Propane)	HC	-187.63	-42.114	96.74	4,251.2	376.85	~20	A3
R1270 (Propylene)	HC	-185.2	-47.619	91.061	4,555	301.85	<20	A3
R14	PFC	-183.61	-128.05	-45.64	3,750	349.85	7,390	A1
R170 (Ethane)	HC	-182.78	-88.581	32.172	4,872.2	401.85	~20	A3
R50 (Methane)	HC	-182.46	-161.48	-82.586	4,599.2	351.85	23	A3
R1150 (Ethylene)	HC	-169.16	-103.77	9.2	5,041.8	176.85	<20	A3
R600a (Isobutane)	HC	-159.42	-11.749	134.66	3,629	301.85	~20	A3
R23	HFC	-155.13	-82.018	26.143	4,832	201.85	14,200	A1
R218	PFC	-147.7	-36.79	71.87	2,640	166.85	8,830	A1
R41	HFC	-143.33	-78.31	44.13	5,897	151.85	107	n.d.
R600 (Butane)	HC	-138.26	-0.49	151.98	3,796	301.85	~20	A3
R32	HFC	-136.81	-51.651	78.105	5,782	161.85	716	A2L
R152a	HFC	-118.59	-24.023	113.26	4,516.8	226.85	133	A2
R143a	HFC	-111.81	-47.241	72.707	3,761	376.85	4,180	A2L
R1234ze(E)	HFO	-104.53	-18.973	109.36	3,634.9	146.85	6	A2L
R134a	HFC	-103.3	-26.074	101.06	4,059.3	181.85	1,370	A1
R125	HFC	-100.63	-48.09	66.023	3,617.7	226.85	3,420	A1
R116	PFC	-100.05	-78.09	19.88	3,048	151.85	12,200	A1
R717 (Ammonia)	I.C.	-77.655	-33.327	132.25	11,333	426.85	<1	B2L
R507A	HFC blend	-73.15 [a]	-46.74	70.615	3,704.9	226.85	3,800	A1
R404A	HFC blend	-73.15 [a]	-46.22	72.12	3,734.8	226.85	3,700	A1
R407C	HFC blend	-73.15 [a]	-43.63	86.195	4,631.7	226.85	1,700	A1
R410A	HFC blend	-73.15 [a]	-51.44	71.344	4,901.2	226.85	2,100	A1
R744 (Carbon dioxide)	I.C.	-56.558	-78.464	30.978	7,377.3	1726.85	1	A1
R1234yf	HFO	-53.15 [a]	-29.45	94.7	3,382.2	136.85	<4.4	A2L
R718 (Water)	I.C.	0.01	99.974	373.95	22,064	1726.85	<1	A1

[a] Limit of EoS in NIST REFPROP [51] database; [b] GWP 100 years [52]; [c] ANSI/ASHRAE Standard 34 [53].

Nomenclature: I.C. – Inorganic compound; HC – Hydrocarbon; HFC – Hydrofluorocarbon; PFC – Perfluorocarbon; HFO – Hydrofluoro-Olefin.

Table 3. Performance results of each candidate fluid for the DC network and power cycle RC-2: Pipe size, working pressures, pressure and temperature drop, latent heat of vaporization, density and dynamic viscosity.

Fluid	Pipe size (DN)		Pressure, kPa		$\Delta P/L$, (kPa/km)		ΔT, °C		Δh_v, kJ/kg		ρ, kg/m^3		μ, μPa·s	
	S	R	P_{19}	P_{22}	S	R	S	R	-30°C	-50°C	ρ_{19}	ρ_{22}	μ_{19}	μ_{22}
CO_2	150	450	854	1874	223	85.6	0.6	1.4	303.5	339.7	17.6	1155	13.8	229
R23	200	500	677	1227	108	98.6	0.6	0.4	184.9	208.4	21.3	1308	14.3	186
R32	150	900	131	648	187	10.6	0.9	1.6	356.8	380.1	3.2	1208	11.0	278
R116	200	550	591	1311	274	112	0.5	-9	89.9	102.5	35.2	1475	15.1	173
Ethane	200	500	650	1200	67.8	48.9	0.6	0.8	388.9	429.8	8.9	492	8.9	105
Ethylene	200	400	1273	2107	85.0	105	0.6	0.9	327.7	383.6	17.0	481	17.0	94
R41	200	600	439	1189	186	25.8	0.8	1.4	407.0	444.4	7.1	819	11.8	162
R410A	200	900	136	843	287	23.4	0.7	1.3	153.5	271.6	4.4	1345	11.4	311

S: Supply pipeline (liquid) with a design velocity of 1.5 – 2.5 m/s.

R: Return pipeline (superheated vapor) with a design velocity of 20 – 25 m/s.

Table 4. Performance indicators of the LNG regasification process without exergy recovery and the obtained by the polygeneration plant proposed when operating with the selected working fluids and heat transfer fluids (Power cycle RC1 – Methane; DC + Power cycle RC2 – CO_2; Power cycle RC3 – Propane) for an LNG regasification capacity of 180 t/h.

Operation mode	**Performance indicators**						
	$\dot{W}_{net}$, **MW**	**DCS, MW**	**EEP, kWh/t-LNG**	**PES [a], GWh/y**	**SW, t-SW/t-LNG**	**ACO$_2$e [b], t-CO$_2$/y**	η_{ex}, **%**
LNG regasification without exergy recovery	-1.1	0	-6.2	-19	38.7	+3,691	0
Polygeneration plant with exergy recovery	**13.2**	**16.4**	**125.3**	**380**	**14.9**	**-75,079**	**40.6**
- Power cycle RC-1	1.8	-	9.9	30	5.7	-5,949	35.2
- DC + power cycle RC-2	1.0	16.4	57.3	174	-	-34,355	28.8
- Power cycle RC-3	7.5	-	41.8	127	-	-25,033	44.4
- NG direct expansion unit	2.9	-	16.3	49	9.2	-9,742	62.7

[a] Taking as a reference an efficiency of 52%

[b] Considering an emission factor of 0.380 kg-CO_2/kWh

Table A1. Energy and exergy balance equations of all the components of the polygeneration plant.

Component	Energy balance	Exergy balance
Condenser C-1	$\dot{Q}_{C1} = \dot{m}_{LNG}(h_3 - h_2) = \dot{m}_{RC1}(h_{13} - h_{14})$	$\dot{I}_{C1} = \dot{E}x_2 + \dot{E}x_{13} - \dot{E}x_3 - \dot{E}x_{14}$
Condenser C-2	$\dot{Q}_{C2} = \dot{m}_{LNG}(h_4 - h_3) = \dot{m}_{DC\&RC2}(h_{20} - h_{21})$	$\dot{I}_{C2} = \dot{E}x_3 + \dot{E}x_{20} - \dot{E}x_4 - \dot{E}x_{21}$
Condenser C-3	$\dot{Q}_{C3} = \dot{m}_{LNG}(h_5 - h_4) = \dot{m}_{RC3}(h_{44} - h_{45})$	$\dot{I}_{C3} = \dot{E}x_4 + \dot{E}x_{44} - \dot{E}x_5 - \dot{E}x_{45}$
Heater H-1	$\dot{Q}_{H1} = \dot{m}_{RC1}(h_9 - h_{16}) + \dot{m}_{RC1}(h_{11} - h_{10}) = \dot{m}_{SW,H1}(h_{17} - h_{18})$	$\dot{I}_{H1} = \dot{E}x_{10} + \dot{E}x_{16} + \dot{E}x_{17} - \dot{E}x_9 - \dot{E}x_{11} - \dot{E}x_{18}$
Heater H-2	$\dot{Q}_{H2} = \dot{m}_{DC\&RC2}(h_{31} - h_{30}) = \dot{m}_{WH}(h_{38} - h_{39})$	$\dot{I}_{H2} = \dot{E}x_{30} + \dot{E}x_{38} - \dot{E}x_{31} - \dot{E}x_{39}$
Heater H-3	$\dot{Q}_{H3} = \dot{m}_{RC3}(h_{40} - h_{47}) + \dot{m}_{RC3}(h_{42} - h_{41})$	$\dot{I}_{H3} = \dot{E}x_{41} + \dot{E}x_{47} + \dot{Q}_{H3}\left(1 - \frac{T_0}{T_{bb}}\right) - \dot{E}x_{40} - \dot{E}x_{42}$
Heater H-4	$\dot{Q}_{H4} = \dot{m}_{LNG}(h_6 - h_5) = \dot{m}_{SW,H4}(h_{48} - h_{49})$	$\dot{I}_{H4} = \dot{E}x_5 + \dot{E}x_{48} - \dot{E}x_6 - \dot{E}x_{49}$
Heater H-5	$\dot{Q}_{H5} = \dot{m}_{LNG}(h_8 - h_7) = \dot{m}_{SW,H5}(h_{50} - h_{51})$	$\dot{I}_{H5} = \dot{E}x_7 + \dot{E}x_{50} - \dot{E}x_8 - \dot{E}x_{51}$
Pump P1	$\dot{W}_{P1} = \dot{m}_{LNG}(h_2 - h_1)$	$\dot{I}_{P1} = \dot{E}x_1 + \dot{W}_{P1} - \dot{E}x_2$
Pump P2	$\dot{W}_{P2} = \dot{m}_{RC1}(h_{15} - h_{14})$	$\dot{I}_{P2} = \dot{E}x_{14} + \dot{W}_{P2} - \dot{E}x_{15}$
Pump P3	$\dot{W}_{P3} = \dot{m}_{DC\&RC2}(h_{22} - h_{21})$	$\dot{I}_{P3} = \dot{E}x_{21} + \dot{W}_{P3} - \dot{E}x_{22}$
Pump P4	$\dot{W}_{P4} = \dot{m}_{RC3}(h_{46} - h_{45})$	$\dot{I}_{P4} = \dot{E}x_{45} + \dot{W}_{P4} - \dot{E}x_{46}$
Recuperator R-1	$\dot{Q}_{R1} = \dot{m}_{RC1}(h_{12} - h_{13}) = \dot{m}_{RC1}(h_{16} - h_{15})$	$\dot{I}_{R1} = \dot{E}x_{12} + \dot{E}x_{15} - \dot{E}x_{13} - \dot{E}x_{16}$
Recuperator R-2	$\dot{Q}_{R2} = \dot{m}_{RC3}(h_{43} - h_{44}) = \dot{m}_{RC3}(h_{47} - h_{46})$	$\dot{I}_{R2} = \dot{E}x_{43} + \dot{E}x_{46} - \dot{E}x_{44} - \dot{E}x_{47}$
Turbine T1 (HP)	$\dot{W}_{T1-HP} = \dot{m}_{RC1}(h_9 - h_{10})$	$\dot{I}_{T1-HP} = \dot{E}x_9 - \dot{E}x_{10} - \dot{W}_{T1-HP}$
Turbine T1 (LP)	$\dot{W}_{T1-LP} = \dot{m}_{RC1}(h_{11} - h_{12})$	$\dot{I}_{T1-LP} = \dot{E}x_{11} - \dot{E}x_{12} - \dot{W}_{T1-LP}$
Turbine T2	$\dot{W}_{T2} = \dot{m}_{DC\&RC2}(h_{31} - h_{19})$	$\dot{I}_{T2} = \dot{E}x_{31} - \dot{E}x_{19} - \dot{W}_{T2}$
Turbine T3 (HP)	$\dot{W}_{T3-HP} = \dot{m}_{RC3}(h_{40} - h_{41})$	$\dot{I}_{T3-HP} = \dot{E}x_{40} - \dot{E}x_{41} - \dot{W}_{T3-HP}$
Turbine T3 (LP)	$\dot{W}_{T3-LP} = \dot{m}_{RC3}(h_{42} - h_{43})$	$\dot{I}_{T3-LP} = \dot{E}x_{42} - \dot{E}x_{43} - \dot{W}_{T3-LP}$
NG Expander (EXP)	$\dot{W}_{EXP} = \dot{m}_{LNG}(h_6 - h_7)$	$\dot{I}_{EXP} = \dot{E}x_6 - \dot{E}x_7 - \dot{W}_{EXP}$

Table A2. Thermodynamic data of each state point of the polygeneration plant when operating with the selected working fluids and heat transfer fluids (Power cycle RC-1 – Methane; DC + power cycle RC-2 – CO_2; Power cycle RC-3 – Propane).

Nº	Fluid	$\dot{m}$, t/h	T, °C	p, MPa	h, kJ/kg	s, kJ/(kg·K)	Nº	Fluid	$\dot{m}$, t/h	T, °C	p, MPa	h, kJ/kg	s, kJ/(kg·K)
1	LNG	180.0	-162.0	0.13	-912.68	-6.693	27	CO_2	69.1	-30.0	1.43	-69.96	-0.741
2	LNG	180.0	-158.6	7.20	-890.50	-6.644	28	CO_2	17.3	-48.8	1.43	-411.33	-2.151
3	LNG	180.0	-135.0	7.20	-807.98	-5.990	29	CO_2	17.3	-30.0	1.43	-69.96	-0.741
4	NG	180.0	-65.0	7.20	-437.55	-3.904	30	CO_2	172.8	-30.0	1.43	-69.96	-0.741
5	NG	180.0	-15.0	7.20	-189.79	-2.813	31	CO_2	172.8	30.0	1.43	-9.27	-0.517
6	NG	180.0	5.0	7.20	-129.39	-2.588	32	NH_3	21.9	-25.0	0.15	1430.62	5.983
7	NG	180.0	-47.8	3.00	-210.10	-2.524	33	NH_3	21.9	-25.0	0.15	86.12	0.564
8	NG	180.0	5.0	3.00	-78.24	-1.997	34	NH_3	18.2	-10.0	0.29	1450.66	5.757
9	Methane	31.0	10.0	10.53	-153.95	-2.838	35	NH_3	18.2	-10.0	0.29	153.95	0.829
10	Methane	31.0	-62.1	3.20	-253.98	-2.754	36	Water	200.7	12.0	0.10	50.51	0.181
11	Methane	31.0	10.0	3.20	-68.43	-1.994	37	Water	200.7	5.0	0.10	21.12	0.076
12	Methane	31.0	-66.4	0.75	-210.42	-1.870	38	Water	501.7	40.0	0.10	167.62	0.572
13	Methane	31.0	-112.9	0.75	-316.90	-2.454	39	Water	501.7	35.0	0.10	146.72	0.505
14	Methane	31.0	-130.0	0.75	-795.53	-5.781	40	Propane	102.6	300.0	18.15	1131.22	3.142
15	Methane	31.0	-122.9	10.53	-760.82	-5.723	41	Propane	102.6	221.2	3.39	1011.31	3.185
16	Methane	31.0	-95.2	10.53	-654.34	-5.074	42	Propane	102.6	300.0	3.39	1233.05	3.601
17	Seawater	1017.0	20.0	0.30	84.19	0.296	43	Propane	102.6	221.9	0.35	1045.98	3.669
18	Seawater	1017.0	15.0	0.30	63.27	0.224	44	Propane	102.6	17.3	0.35	609.95	2.552
19	CO_2	172.8	-0.4	0.85	-31.26	-0.503	45	Propane	102.6	-10.0	0.35	175.20	0.908
20	CO_2	172.8	1.0	0.68	-27.89	-0.450	46	Propane	102.6	2.3	18.15	218.28	0.948
21	CO_2	172.8	-50.0	0.68	-413.85	-2.160	47	Propane	102.6	158.4	18.15	654.31	2.187
22	CO_2	172.8	-49.5	1.88	-412.48	-2.158	48	Seawater	519.5	20.0	0.30	84.19	0.296
23	CO_2	172.8	-48.8	1.43	-411.33	-2.151	49	Seawater	519.5	15.0	0.30	63.27	0.224
24	CO_2	86.4	-48.8	1.43	-411.33	-2.151	50	Seawater	1134.0	20.0	0.30	84.19	0.296
25	CO_2	86.4	-30.0	1.43	-69.96	-0.741	51	Seawater	1134.0	15.0	0.30	63.27	0.224
26	CO_2	69.1	-48.8	1.43	-411.33	-2.151							

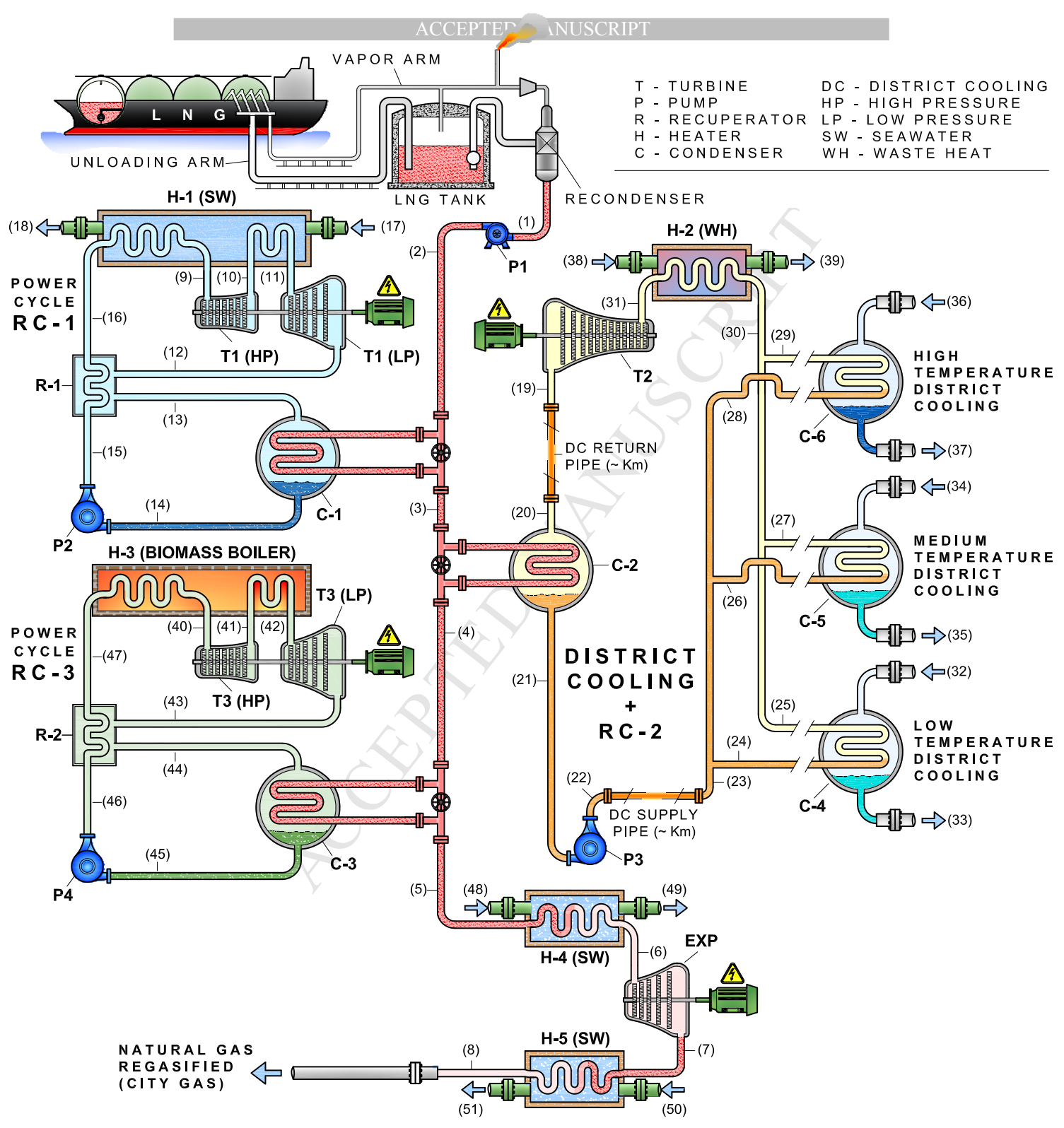

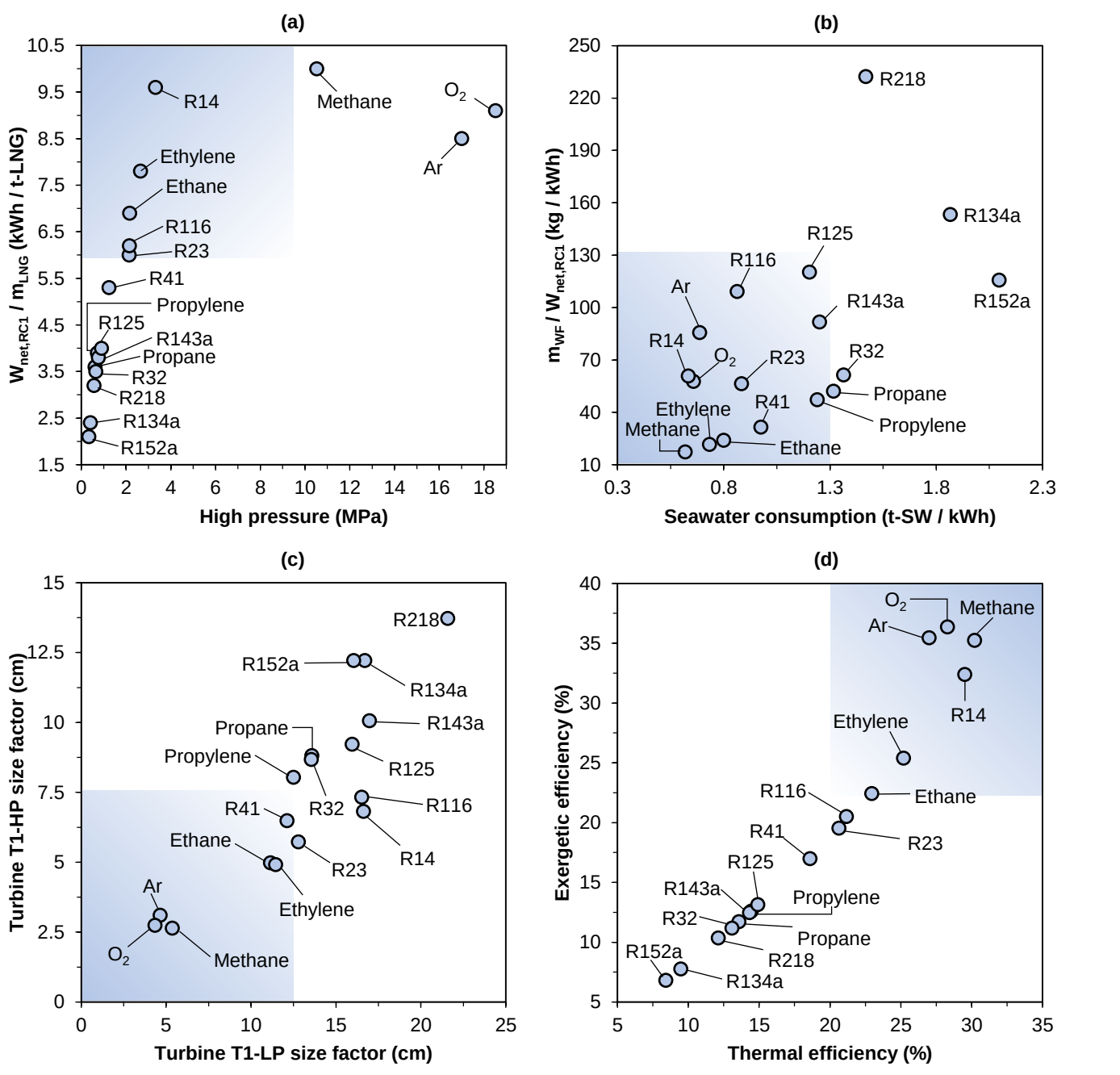
(a)
$W_{net,RC1}$ / m_{LNG} (kWh / t-LNG)
High pressure (MPa)
R14
Methane
O_2
Ar
Ethylene
Ethane
R116
R23
R41
Propylene
R125
R143a
Propane
R32
R218
R134a
R152a
(b)
m_{WF} / $W_{net,RC1}$ (kg / kWh)
Seawater consumption (t-SW / kWh)
R218
R134a
R125
R116
Ar
R143a
R152a
R14
O_2
R23
R32
Propane
Ethylene
R41
Propylene
Methane
Ethane
(c)
Turbine T1-HP size factor (cm)
Turbine T1-LP size factor (cm)
R218
R152a
R134a
Propane
R143a
Propylene
R125
R32
R116
R41
Ethane
R14
R23
Ar
Ethylene
O_2
Methane
(d)
Exergetic efficiency (%)
Thermal efficiency (%)
O_2
Methane
Ar
R14
Ethylene
R116
Ethane
R41
R23
R125
R143a
Propylene
R32
Propane
R152a
R218
R134a

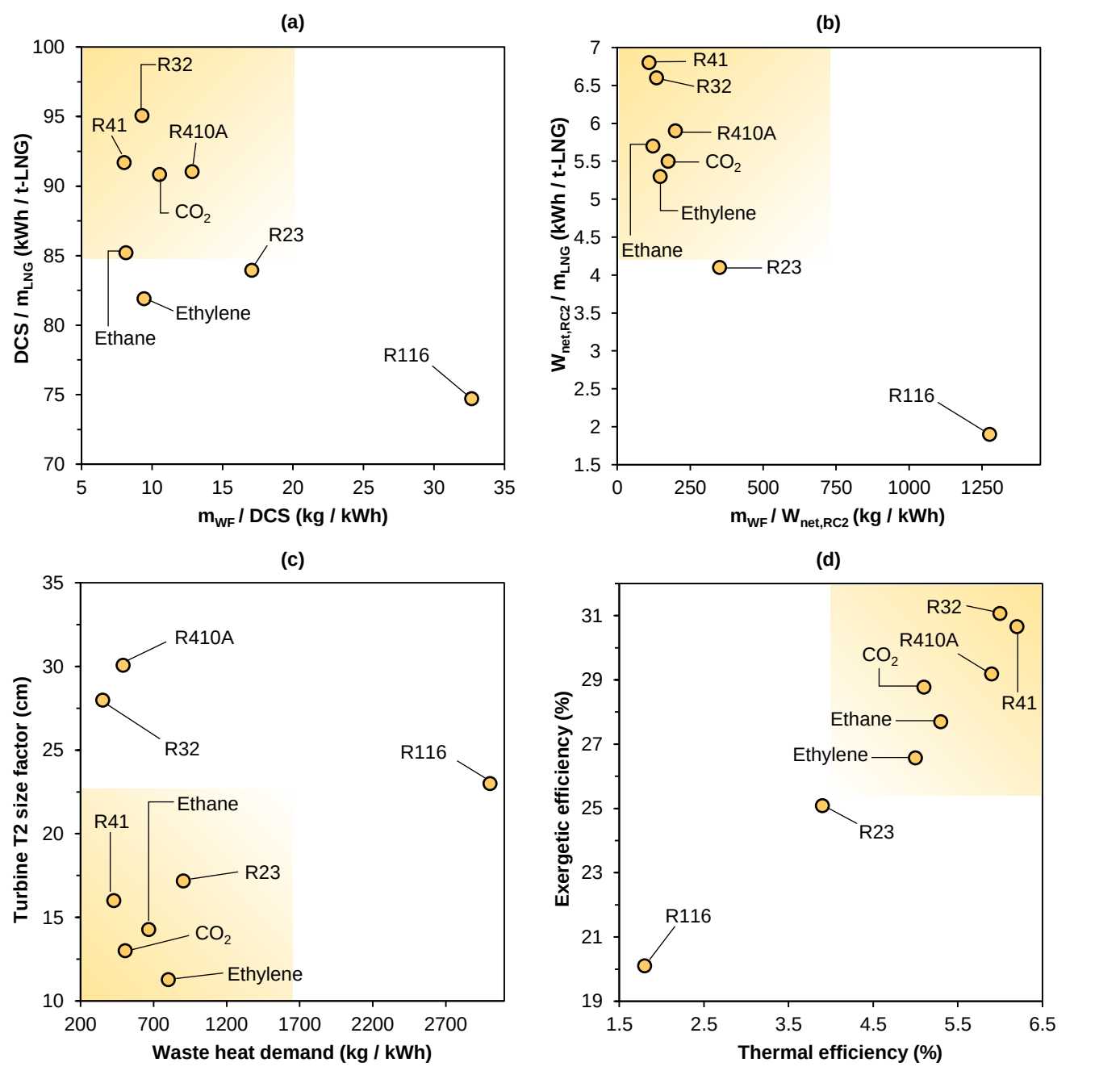
(a)
DCS / m_LNG (kWh / t-LNG)
m_WF / DCS (kg / kWh)
R32
R41
R410A
CO2
R23
Ethylene
Ethane
R116
(b)
W_net,RC2 / m_LNG (kWh / t-LNG)
m_WF / W_net,RC2 (kg / kWh)
R41
R32
R410A
CO2
Ethylene
Ethane
R23
R116
(c)
Turbine T2 size factor (cm)
Waste heat demand (kg / kWh)
R410A
R32
R116
Ethane
R41
R23
CO2
Ethylene
(d)
Exergetic efficiency (%)
Thermal efficiency (%)
R32
R410A
CO2
R41
Ethane
Ethylene
R23
R116

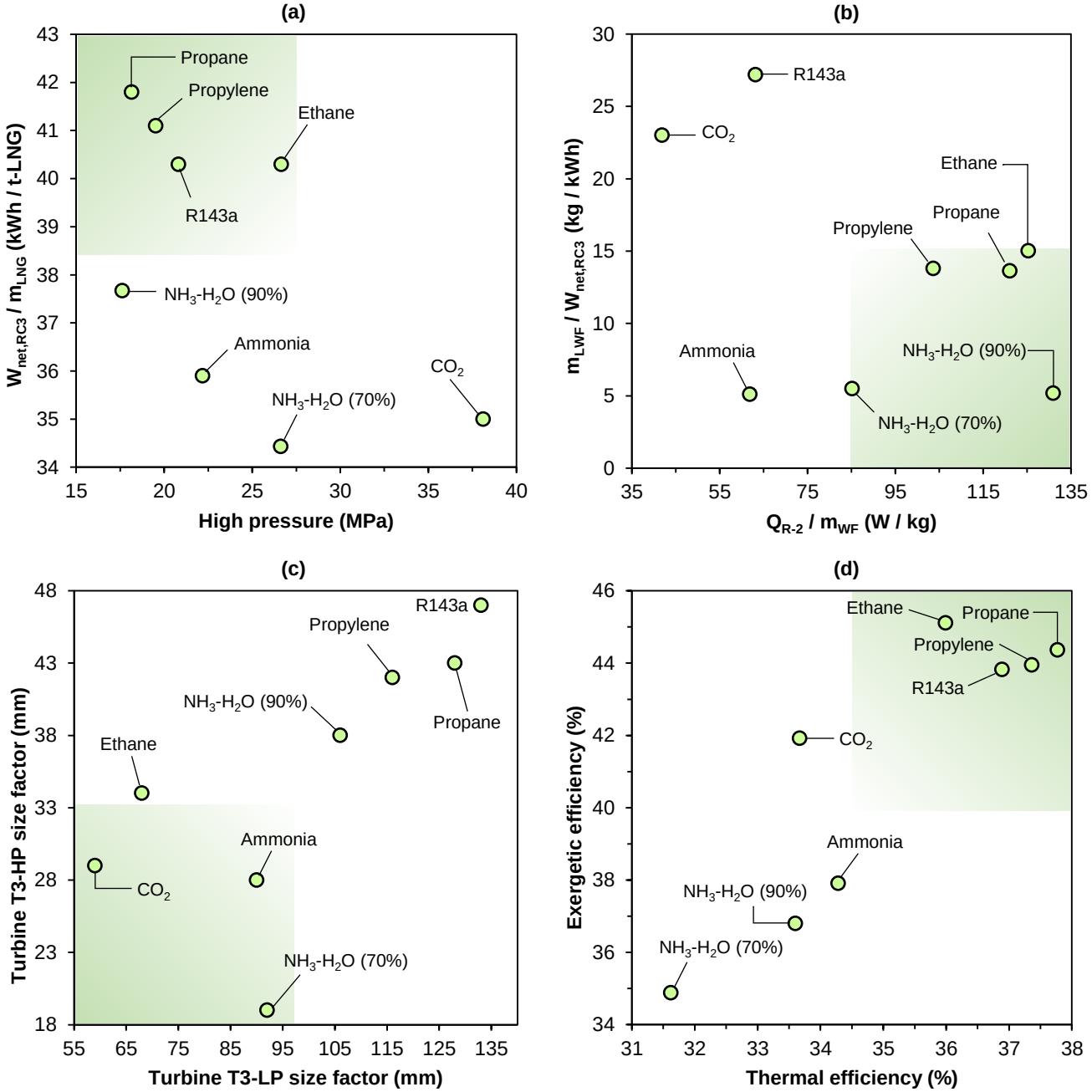
(a)
Propane
Propylene
Ethane
R143a
NH3-H2O (90%)
Ammonia
CO2
NH3-H2O (70%)
Wnet,RC3 / mLNG (kWh / t-LNG)
High pressure (MPa)
(b)
R143a
CO2
Ethane
Propane
Propylene
Ammonia
NH3-H2O (90%)
NH3-H2O (70%)
mLWF / Wnet,RC3 (kg / kWh)
QR-2 / mWF (W / kg)
(c)
R143a
Propylene
NH3-H2O (90%)
Propane
Ethane
Ammonia
CO2
NH3-H2O (70%)
Turbine T3-HP size factor (mm)
Turbine T3-LP size factor (mm)
(d)
Ethane
Propane
Propylene
R143a
CO2
Ammonia
NH3-H2O (90%)
NH3-H2O (70%)
Exergetic efficiency (%)
Thermal efficiency (%)

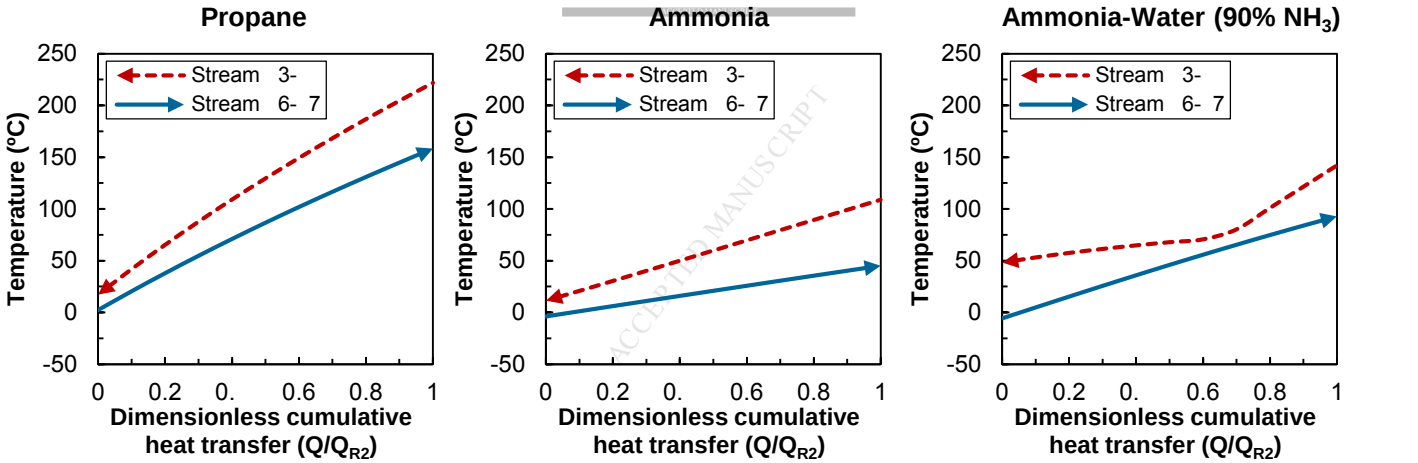
Propane
Ammonia
Ammonia-Water (90% NH3)
Stream 3-
Stream 6- 7
Temperature (ºC)
250
200
150
100
50
0
-50
0
0.2
0.
0.6
0.8
1
Dimensionless cumulative heat transfer (Q/QR2)
ACCEPTED MANUSCRIPT

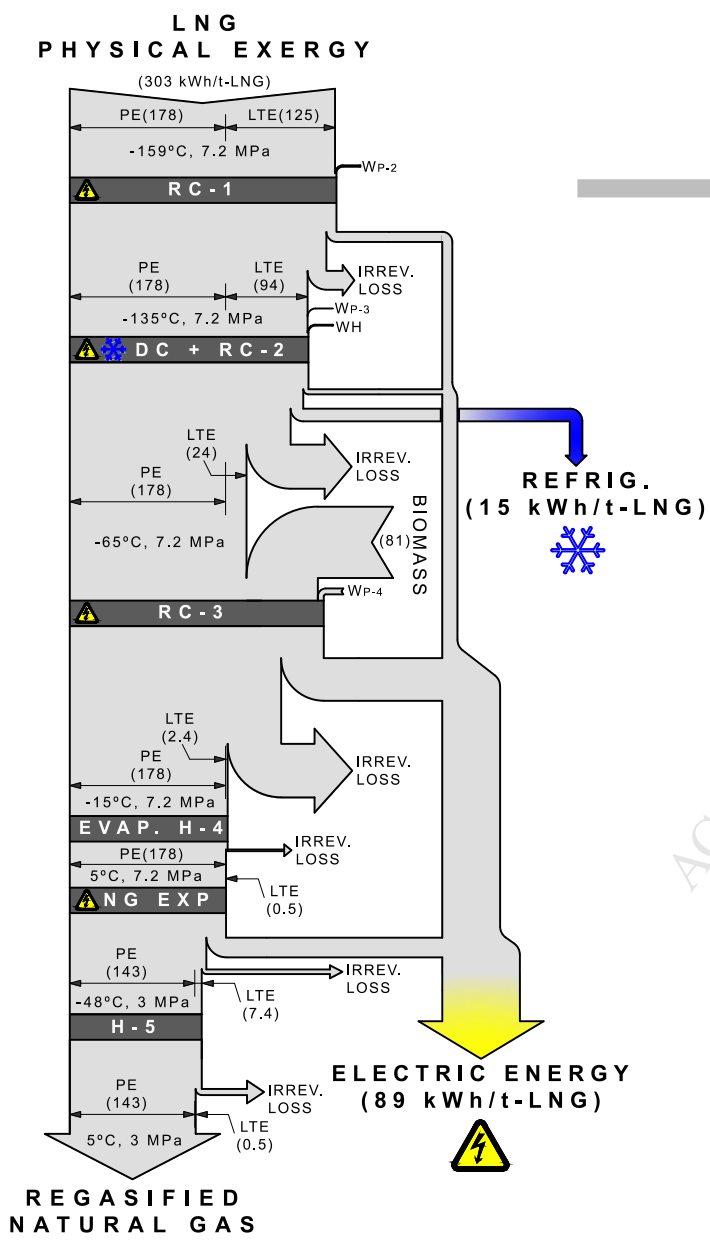
LNG
PHYSICAL EXERGY
(303 kWh/t-LNG)
PE(178)
LTE(125)
-159°C, 7.2 MPa
WP-2
RC-1
PE
(178)
LTE
(94)
IRREV.
LOSS
-135°C, 7.2 MPa
WP-3
WH
DC + RC-2
LTE
(24)
PE
(178)
IRREV.
LOSS
REFRIG.
(15 kWh/t-LNG)
-65°C, 7.2 MPa
(81)
BIOMASS
WP-4
RC-3
LTE
(2.4)
PE
(178)
IRREV.
LOSS
-15°C, 7.2 MPa
EVAP. H-4
IRREV.
LOSS
PE(178)
5°C, 7.2 MPa
LTE
(0.5)
NG EXP
PE
(143)
IRREV.
LOSS
-48°C, 3 MPa
LTE
(7.4)
H-5
ELECTRIC ENERGY
(89 kWh/t-LNG)
PE
(143)
IRREV.
LOSS
LTE
(0.5)
5°C, 3 MPa
REGASIFIED
NATURAL GAS

CE: Chemical exergy
LTE: Low-Temperature exergy
PE: Pressure exergy

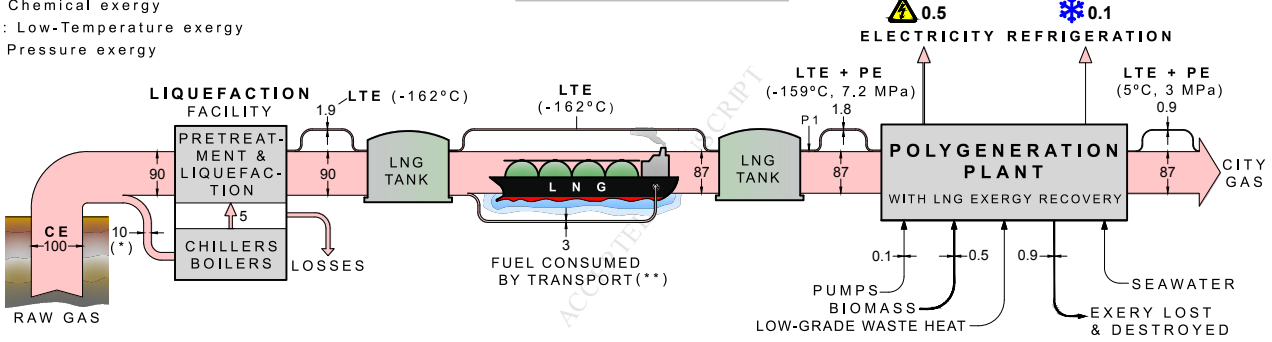

(*) The liquefaction facility consumes approximately 10% of the total gas treated.

(**) LNG transport Qatar-Tokyo for an LNG ship of 160,000 m^3. Fuel consumption of 72 t-LNG/day and average speed of 19 knots.

Highlights

- Physical exergy of Liquefied Natural Gas (LNG) is exploited via polygeneration.
- Operating fluids are selected for a polygeneration plant that exploits LNG exergy.
- The selected fluids are natural: Methane, CO_2 and propane.
- The plant regasifies 180 t-LNG/h producing 125 kWh/t-LNG of equivalent electricity.
- The exergy efficiency of the polygeneration plant modelled in this paper is 40.6%.